ESCUELA TÉCNICA SUPERIOR DE INGENIERÍA (ICAI)

INGENIERO INDUSTRIAL

ANÁLISIS ESTRUCTURAL DEL SOPORTE DE UNA BARRA DE COMBUSTIBLE DE UN ELEMENTO DE COMBUSTIBLE DE UN PWR BAJO IRRADIACIÓN USANDO EL MÉTODO DE ELEMENTOS FINITOS

Autor: Ana Alós Díez
Director: Prof. Dr. Rafael Macián Juan

Madrid
Mayo de 2015

AUTORIZACIÓN PARA LA DIGITALIZACIÓN, DEPÓSITO Y DIVULGACIÓN EN ACCESO *ABIERTO* (*RESTRINGIDO*) DE DOCUMENTACIÓN

1º. Declaración de la autoría y acreditación de la misma.

El autor D. ANA ALÓS DÍEZ , como ALUMNA de la UNIVERSIDAD PONTIFICIA COMILLAS (COMILLAS), **DECLARA**

que es el titular de los derechos de propiedad intelectual, objeto de la presente cesión, en relación con la obra PROYECTO FIN DE CARRERA: ANÁLISIS ESTRUCTURAL DEL SOPORTE DE UNA BARRA DE COMBUSTIBLE DE UN PWR BAJO IRRADIACIÓN USANDO EL FEM, que ésta es una obra original, y que ostenta la condición de autor en el sentido que otorga la Ley de Propiedad Intelectual como titular único o cotitular de la obra.

En caso de ser cotitular, el autor (firmante) declara asimismo que cuenta con el consentimiento de los restantes titulares para hacer la presente cesión. En caso de previa cesión a terceros de derechos de explotación de la obra, el autor declara que tiene la oportuna autorización de dichos titulares de derechos a los fines de esta cesión o bien que retiene la facultad de ceder estos derechos en la forma prevista en la presente cesión y así lo acredita.

2º. Objeto y fines de la cesión.

Con el fin de dar la máxima difusión a la obra citada a través del Repositorio institucional de la Universidad y hacer posible su utilización de *forma libre y gratuita* (*con las limitaciones que más adelante se detallan*) por todos los usuarios del repositorio y del portal e-ciencia, el autor **CEDE** a la Universidad Pontificia Comillas de forma gratuita y no exclusiva, por el máximo plazo legal y con ámbito universal, los derechos de digitalización, de archivo, de reproducción, de distribución, de comunicación pública, incluido el derecho de puesta a disposición electrónica, tal y como se describen en la Ley de Propiedad Intelectual. El derecho de transformación se cede a los únicos efectos de lo dispuesto en la letra (a) del apartado siguiente.

3º. Condiciones de la cesión.

Sin perjuicio de la titularidad de la obra, que sigue correspondiendo a su autor, la cesión de derechos contemplada en esta licencia, el repositorio institucional podrá:

[1] Especificar si es una tesis doctoral, proyecto fin de carrera, proyecto fin de Máster o cualquier otro trabajo que deba ser objeto de evaluación académica

(a) Transformarla para adaptarla a cualquier tecnología susceptible de incorporarla a internet; realizar adaptaciones para hacer posible la utilización de la obra en formatos electrónicos, así como incorporar metadatos para realizar el registro de la obra e incorporar "marcas de agua" o cualquier otro sistema de seguridad o de protección.

(b) Reproducirla en un soporte digital para su incorporación a una base de datos electrónica, incluyendo el derecho de reproducir y almacenar la obra en servidores, a los efectos de garantizar su seguridad, conservación y preservar el formato. .

(c) Comunicarla y ponerla a disposición del público a través de un archivo abierto institucional, accesible de modo libre y gratuito a través de internet.[2]

(d) Distribuir copias electrónicas de la obra a los usuarios en un soporte digital. [3]

4º. Derechos del autor.

El autor, en tanto que titular de una obra que cede con carácter no exclusivo a la Universidad por medio de su registro en el Repositorio Institucional tiene derecho a:

a) A que la Universidad identifique claramente su nombre como el autor o propietario de los derechos del documento.

b) Comunicar y dar publicidad a la obra en la versión que ceda y en otras posteriores a través de cualquier medio.

c) Solicitar la retirada de la obra del repositorio por causa justificada. A tal fin deberá ponerse en contacto con el vicerrector/a de investigación (curiarte@rec.upcomillas.es).

d) Autorizar expresamente a COMILLAS para, en su caso, realizar los trámites necesarios para la obtención del ISBN.

---

[2] En el supuesto de que el autor opte por el acceso restringido, este apartado quedaría redactado en los siguientes términos:

(c) Comunicarla y ponerla a disposición del público a través de un archivo institucional, accesible de modo restringido, en los términos previstos en el Reglamento del Repositorio Institucional

[3] En el supuesto de que el autor opte por el acceso restringido, este apartado quedaría eliminado.

d) Recibir notificación fehaciente de cualquier reclamación que puedan formular terceras personas en relación con la obra y, en particular, de reclamaciones relativas a los derechos de propiedad intelectual sobre ella.

5º. Deberes del autor.

El autor se compromete a:

a) Garantizar que el compromiso que adquiere mediante el presente escrito no infringe ningún derecho de terceros, ya sean de propiedad industrial, intelectual o cualquier otro.

b) Garantizar que el contenido de las obras no atenta contra los derechos al honor, a la intimidad y a la imagen de terceros.

c) Asumir toda reclamación o responsabilidad, incluyendo las indemnizaciones por daños, que pudieran ejercitarse contra la Universidad por terceros que vieran infringidos sus derechos e intereses a causa de la cesión.

d) Asumir la responsabilidad en el caso de que las instituciones fueran condenadas por infracción de derechos derivada de las obras objeto de la cesión.

6º. Fines y funcionamiento del Repositorio Institucional.

La obra se pondrá a disposición de los usuarios para que hagan de ella un uso justo y respetuoso con los derechos del autor, según lo permitido por la legislación aplicable, y con fines de estudio, investigación, o cualquier otro fin lícito. Con dicha finalidad, la Universidad asume los siguientes deberes y se reserva las siguientes facultades:

a) Deberes del repositorio Institucional:

- La Universidad informará a los usuarios del archivo sobre los usos permitidos, y no garantiza ni asume responsabilidad alguna por otras formas en que los usuarios hagan un uso posterior de las obras no conforme con la legislación vigente. El uso posterior, más allá de la copia privada, requerirá que se cite la fuente y se reconozca la autoría, que no se obtenga beneficio comercial, y que no se realicen obras derivadas.

- La Universidad no revisará el contenido de las obras, que en todo caso permanecerá bajo la responsabilidad exclusiva del autor y no estará obligada a ejercitar acciones legales en nombre del autor en el supuesto de infracciones a derechos de propiedad intelectual derivados del depósito y archivo de las obras. El autor renuncia a cualquier reclamación frente a la Universidad por las formas no ajustadas a la legislación vigente en que los usuarios hagan uso de las obras.

- La Universidad adoptará las medidas necesarias para la preservación de la obra en un futuro.

b) Derechos que se reserva el Repositorio institucional respecto de las obras en él registradas:

- retirar la obra, previa notificación al autor, en supuestos suficientemente justificados, o en caso de reclamaciones de terceros.

Madrid, a 26 de Mayo de 2015

ACEPTA

Fdo.....

Proyecto realizado por el alumno/a:

Ana Alós Díez

Fdo.: ..... Fecha: 19 / 05 / 2015

Autorizada la entrega del proyecto cuya información no es de carácter confidencial

EL DIRECTOR DEL PROYECTO

Rafael Macián Juan

Fdo.: ..... Fecha: 19 / 05 / 2015

Vº Bº del Coordinador de Proyectos

(poner el nombre del Coordinador de Proyectos)

Fdo.: ..... Fecha: ...../ ...../ .....

ESCUELA TÉCNICA SUPERIOR DE INGENIERÍA (ICAI)

INGENIERO INDUSTRIAL

ANÁLISIS ESTRUCTURAL DEL SOPORTE DE UNA BARRA DE COMBUSTIBLE DE UN ELEMENTO DE COMBUSTIBLE DE UN PWR BAJO IRRADIACIÓN USANDO EL MÉTODO DE ELEMENTOS FINITOS

Autor: Ana Alós Díez
Director: Prof. Dr. Rafael Macián Juan

Madrid
Mayo de 2015

ANÁLISIS ESTRUCTURAL DEL SOPORTE DE UNA BARRA DE COMBUSTIBLE DE UN ELEMENTO DE COMBUSTIBLE DE UN PWR BAJO IRRADIACIÓN USANDO EL MÉTODO DE ELEMENTOS FINITOS

Autor: Ana Alós Díez

Director del proyecto: Prof. Dr. Rafael Macián-Juan

Entidad colaboradora: TUM - Technische Universität München, Lehrstuhl für Nukleartechnik

RESUMEN DEL PROYECTO

1. Introducción

El reactor de agua a presión (PWR por sus siglas en inglés) es uno de los tipos de reactores nucleares más utilizados a nivel mundial. La característica principal de este tipo de reactores es que el flujo de agua del circuito primario se mantiene a alta presión, de tal forma que se evita la ebullición dentro de la vasija del reactor.

El análisis del arqueamiento (deformación) es un campo activo de investigación en la ingeniería nuclear debido a su importante impacto sobre el rendimiento de los reactores. Debido a la aparición de momentos flectores, puede aparecer el contacto de los elementos de combustible vecinos causando de esta manera el desgaste en las rejillas espaciadoras. Así, un arqueamiento excesivo de estos elementos puede provocar tanto problemas de seguridad como operacionales en el reactor. Además, la relajación de los muelles de soporte de una barra de combustible que existen en las celdas de las rejillas espaciadoras tiene un gran impacto en el arqueamiento de un FA.

Sin embargo, dado que en el arqueamiento del elemento de combustible intervienen muchos procesos diferentes, este fenómeno es difícil de predecir. Por esa razón, algunos modelos computacionales han sido creados en los últimos años para analizar el arqueamiento del elemento de combustible (FA). El objetivo de este trabajo es implementar un modelo fiable de la conexión existente entre la barra de combustible y la rejilla espaciadora, que gobierna el comportamiento mecánico del elemento de combustible.

Para estudiar el comportamiento mecánico de dicha conexión, se ha implementado un modelo de elementos finitos en ANSYS en dos y tres dimensiones. Este proyecto se centra en los aspectos mecánicos estáticos que se relacionan con el soporte de las barras de combustible. El trabajo se divide en dos partes: la primera está dedicada al comportamiento estático rotacional de las barras de combustible dentro de las celdas de las rejillas espaciadoras, y la segunda estudia la relajación de la fuerza de los muelles de soporte durante la irradiación de los elementos de combustible. Para simplificar el problema, se ha considerado los diferentes efectos como procesos aditivos.

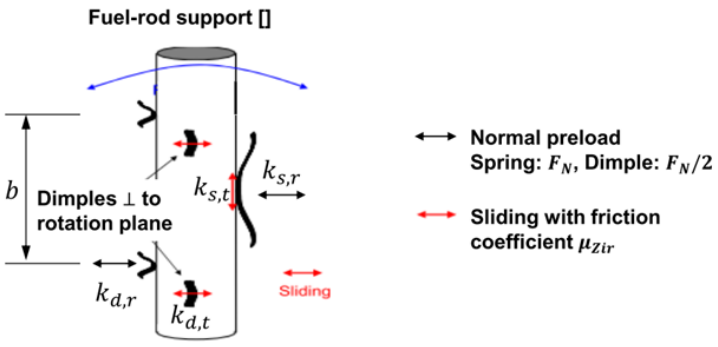

Figura 1. *Representación del mecanismo de rotación de la barra de combustible*

2. Metodología

Implementación del modelo en 2D

El modelo en 2D del soporte de la barra de combustible cosiste en la representación de uno de los dos planos perpendiculares que contiene dos pestañas y un muelle (tal y como se muestra en la *Figura 1*). Sin embargo, el contacto tangencial con los elementos situados en el plano perpendicular también se modela, utilizando un elemento de contacto diferente a los utilizados para los elementos situados en el plano modelado (plano de rotación). La barra de combustible se representa con un elemento viga, la rejilla espaciadora con nodos fijos y las pestañas y muelles con elementos de contacto.

Con el modelo en 2D, se simula la característica rotacional del soporte de la barra de combustible, tanto en carga como en descarga.

Implementación del modelo en 3D

Para el modelo en 3D todas las conexiones entre la barra de combustible y la rejilla espaciadora se modelan usando el mismo tipo de elementos de ANSYS. Sin embargo, la definición de estos elementos varía dependiendo del plano perpendicular en el que estén los elementos modelados.

El modelo en 3D se usa para el análisis rotacional y para el estudio de la relajación de la fuerza de los elementos que mantienen la barra de combustible en su sitio. Además, un test rotacional adicional se lleva a cabo teniendo en cuenta varias precargas axiales, que se aplican como una fuerza puntual en la barra de combustible.

Relajación de la fuerza del muelle durante la operación del reactor debido a la irradiación

Dicha relajación de la fuerza aparece como consecuencia de la ocurrencia de tres procesos fundamentales a medida que el combustible se consume. Para la realización de este estudio se utiliza el modelo implementado en 3D.

- **Disminución del diámetro del revestimiento de la barra de combustible por fluencia lenta:** La diferencia de presión entre el refrigerante que rodea la barra de combustible y la existente en el revestimiento y las pastillas en la barra de combustible crea una fuerza en la superficie del revestimiento dirigida hacia la zona de baja presión, generalmente tensiones radiales hacia el centro de la barra de combustible. Bajo la influencia de estas tensiones, los procesos de fluencia lenta conducen a una reducción plástica del diámetro del revestimiento bajo irradiación (fuel rod creep-down en inglés). Los datos de este proceso se toman de un código externo de comportamiento del combustible.
- **Fluencia lenta por irradiación:** Es una deformación dependiente del tiempo que aparece únicamente bajo la acción de tensiones mecánicas. No obstante, la fluencia lenta por irradiación depende tanto de la tensión aplicada como del flujo de neutrones. En el modelo, este efecto es implementado mediante un algoritmo de integración del tiempo explícita utilizando la fórmula para fluencia lenta por irradiación presentada en *(P.Yvon, 1998)*. Este proceso tiene un efecto en la rigidez del muelle de sujeción.
- **Crecimiento por irradiación:** Es un tipo de deformación a volumen constante que aparece en ausencia de tensiones mecánicas. En el modelo se calcula con la fórmula presentada en *(Billerey, 2004)*.

Normalmente, la relajación de la fuerza de un muelle se modela como la reducción de la rigidez elástica del muelle. Pese a ello, para los elementos de ANSYS que se usan en este modelo, los parámetros de rigidez deben ser constantes. Por eso, la relajación de la fuerza normal se modela moviendo los nodos que representan la rejilla espaciadora una cierta distancia que corresponde con el desplazamiento plástico total. Este desplazamiento es la suma de las deformaciones plásticas debidas a los tres procesos explicados anteriormente, que se suman para cada fase de carga.

3. Resultados

En el estudio en 2D, se observan cuatro fases diferentes durante la rotación en carga (aumentando el momento) de la barra de combustible que corresponden con las fases descritas en estudios previos similares. Para cada fase, el estado del contacto entre la barra de combustible y las pestañas y muelles que lo sujetan coincide con las fases observadas experimentalmente. Además de la rotación en carga, el comportamiento de histéresis de la rotación ha sido también graficado y, tanto la carga como la descarga han sido descritas. Los resultados del modelo concuerdan con los eventos físicos que tienen lugar durante la rotación de la barra de combustible. Por ello, se demuestra la validez del modelo en 2D.

Después del análisis en 2D, el mismo test se llevó a cabo para el modelo en 3D, obteniendo resultados similares. Además, la configuración en 3D fue sometida a la rotación de la barra de combustible alrededor de los dos ejes perpendiculares simultáneamente y la evolución de la rotación es también descrita. En este caso, la curva de carga se parece a la del modelo en 2D, mientras que para la descarga, la curva es considerablemente diferente. Esta diferencia del comportamiento en descarga se debe a la apertura del hueco al final de la etapa de carga en ambos planos perpendiculares. Cuando el hueco está abierto en los dos planos, no hay contacto entre la barra de

combustible y las pestañas, que es el que principalmente rige el comportamiento de histéresis.

El motivo de la realización del test aplicando una precarga axial es que en realidad, los elementos combustibles están sometidos a fuerzas axiales. Por ello, los resultados de este test proporcionan una simulación más realista de la rotación de la barra de combustible. Se observa que, a medida que la fuerza axial se acerca a la máxima fuerza de fricción de la configuración completa, las pendientes de la curva que corresponden con las fases de deslizamiento de la barra de combustible sobre las pestañas y el muelle se suavizan y acortan. La razón es que el aumento de la fuerza axial reduce el margen para el deslizamiento tangencial en las direcciones de los ejes z o y.

La segunda parte del trabajo se diseñó para el estudio de la evolución de la fuerza en el muelle de sujeción de la barra de combustible bajo irradiación, usando el modelo en 3D. En primer lugar, se simuló la relajación de la fuerza del muelle teniendo en cuenta cada uno de los tres procesos más influyentes por separado. Los resultados muestran que el proceso más influyente es la fluencia lenta por irradiación. Sin embargo, al tener en cuenta los tres procesos que afectan a la relajación del muelle, los resultados muestran que, tanto el efecto de la reducción del diámetro del revestimiento de la barra de combustible por fluencia lenta como el crecimiento por irradiación aceleran el proceso de relajación. De acuerdo con los resultados, el muelle estaría completamente relajado tras unas 4000h de operación, tal y como se esperaba. En ese momento, se abriría un hueco entre la barra de combustible y el muelle. La evolución de dicha apertura del hueco se incluye también en el trabajo, así como un análisis paramétrico del efecto de la variación de la rigidez del muelle y del peso del término de fluencia lenta por irradiación.

Todos los resultados presentados y discutidos en este trabajo muestran que, tanto el modelo en 2D como el modelo en 3D del mecanismo de sujeción de la barra de combustible implementados en ANSYS predicen con buena confianza el comportamiento rotacional de la barra de combustible y la relajación de la fuerza del muelle bajo irradiación. Así, y ya que la característica rotacional de las barra de combustible dentro de las rejillas espaciadoras determina la respuesta mecánica de los elementos combustibles a las fuerzas laterales y la relajación de la fuerza normal en los muelles implica una disminución de la rigidez de los elementos combustibles, este modelo debería ser implementado en el modelo completo de los elementos combustibles. El resultado de esta implementación debería permitir al usuario alcanzar soluciones más precisas para el análisis del arqueamiento (deformación) de los elementos combustibles.

Trabajos citados

Billerey, A. (2004). *Evolution of fuel rod support under irradiation - Impact on the mechanical behaviour of fuel assemblies*. Villeurbanne, France.

P.Yvon, J. a. (1998). Irradiation Creep and Growth of Guide Thimble Alloys. France.

STRUCTURAL ANALYSIS OF THE IRRADIATION-INDUCED BEHAVIOR OF THE FUEL-ROD SUPPORT OF A PWR FUEL ASSEMBLY USING THE FINITE ELEMENT MODEL

Author: Ana Alós Díez

Project manager: Prof. Dr. Rafael Macián-Juan

Collaborating entity: TUM - Technische Universität München, Lehrstuhl für Nukleartechnik

PROJECT SUMMARY

1. Introduction

Pressurized Water Reactors (PWRs) are currently the most widely used type of nuclear power plants. The special characteristic of this reactor type is that the water flowing through the first loop is kept at a high pressure, so that boiling inside the reactor is prevented.

Bow analysis is a very concerning issue for nuclear engineering because of its important impact on the performance of the power plant. Due to the appearance of bending moments, neighboring fuel assemblies can contact leading to spacer grid wear. Furthermore, an excessively distorted FA can induce both safety and operational problems for the reactor. Moreover, the relaxation of the springs supporting the fuel rod within a spacer grid cell has an important effect on the bowing of the FA.

However, since bowing involves many different processes, it becomes a challenging issue to predict. For that reason, several computational models have been created over the last years attempting to predict FA bow. The objective of the work which is presented here is to implement a reliable model of the fuel rod to grid connection, which governs the mechanical behavior of the fuel assemblies.

In order to study the mechanical behavior of the fuel rod to spacer grid connection, an ANSYS finite element model in both two and three dimensions has been implemented. This project focuses on the static mechanical aspects concerning the fuel rod support. The work is divided in two different parts: the first one is dedicated to the static rotational behavior of the fuel rod within the grid cell and the second one assesses the relaxation of the spring force during the irradiation of the fuel assemblies. In order to simplify the problem, the different effects are considered as additive processes.

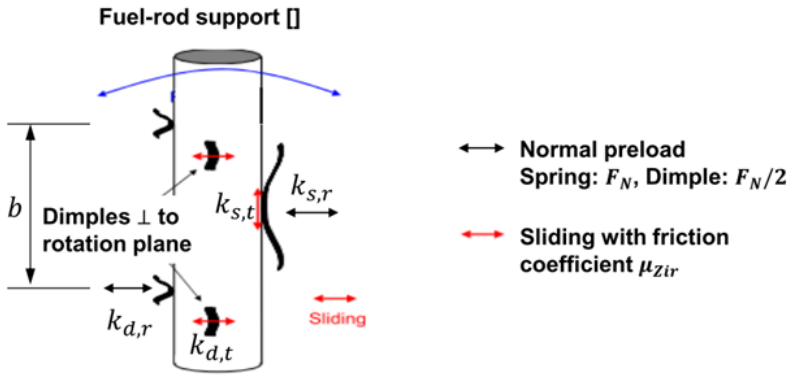

Figure 1. *Fuel rod rotation mechanism representation*

2. Methodology

Implementation of the 2D model

The 2D model of the fuel rod support consists of the representation of one of the two perpendicular planes which contains two dimples and one spring (as shown in *Figure 1*). However, the tangential contact with the elements placed on the perpendicular plane is also modeled by using a contact element, which is different from the contact elements placed on the plane that is modeled (the rotational one). The fuel rod is represented by a beam element, the spacer grid by fixed nodes and the springs and dimples by contact elements.

With the 2D model, the rotational characteristic of the fuel rod support is simulated, both the loading and the unloading.

Implementation of the 3D model

For the 3D model, all the rod-to-grid connections are modeled by using the same type of ANSYS elements. However, their definition varies depending on which perpendicular plane they are located.

The 3D model is used for the rotational behavior analysis and also for the study of the force relaxation of the elements which hold the fuel rod in place. In addition, a rotational test is also carried out taking into account several axial preloads, which are applied as a punctual force to the fuel rod.

Relaxation of the spring force during the operation of the reactor due to irradiation.

This spring force relaxation appears as a consequence of the occurrence of three main processes while the reactor fuel burns. Moreover, this study is done by using the 3D model.

- **Creep-down of the clad diameter:** The difference of pressure between the coolant surrounding the fuel rod and the fuel rod gap creates a force on the clad surface directed towards the low pressure volume, generally inward stresses. Under influence of these stresses, creep processes lead to a plastic decrease of the cladding diameter under irradiation, which is known as fuel rod creep-down. Creep-down data is taken from a fuel performance code.
- **Irradiation creep:** It is a time-dependent deformation type that appears only appears under mechanical stresses. However, irradiation creep depends on both the stress and the neutron flux. In the model, this effect is implemented by following an explicit time integration algorithm and the irradiation creep law presented in *(P.Yvon, 1998)*. This process affects the spring stiffness.
- **Irradiation growth:** It is a volume conservative deformation type that appears in the absence of mechanical stresses. In the model it is calculated with the formula presented in *(Billerey, 2004)*.

Usually the relaxation of the normal force in a spring is modeled as a decrease of the elastic stiffness. Nevertheless, for the ANSYS elements that are used in this model, the stiffness parameters are bound to be constant. Thus, the relaxation of the normal force is modeled by moving the different nodes a certain distance, which will be the total plastic displacement. This displacement is the sum of the plastic deformations due to the three processes that have been already explained that are summed up for every load step.

3. Results

In the 2D study, four different phases during the fuel rod loading rotation have been observed, which correspond with the phases that had already been described by previous studies. For each phase, the state of the contact between the spring and the dimples that support the fuel rod coincides with the rotation phases that have already been experimentally observed. In addition to the rotation loading, the complete hysteretic behavior has been plotted and both the loading and unloading phases of the rotation have been described. The model results show good agreement with the physical events that happen during the fuel rod rotation. Thus, the validity of the 2D model is demonstrated.

After the 2D analysis, the same test was carried out for the 3D model, obtaining similar results. Furthermore, the 3D configuration was also submitted to the rotation of the fuel rod about two perpendicular axes simultaneously and the rotation evolution was described. In this case, the loading curve resembled to the one of the 2D model while the unloading curve was considerably different. This difference of the unloading behavior was due to the gap opening at the end of the loading in both perpendicular planes. When the gap exists in both planes, there is neither sticking nor sliding contact between the fuel rod and the perpendicular dimple which mainly governs the hysteretic behavior.
The reason for the rotational test with an axial preload is that in reality, fuel assemblies are submitted to axial forces so the results of this test provided a more realistic simulation of the fuel rod rotation. It was observed that, as the axial preload was closer to the maximum frictional force for the whole configuration, the slopes of the curve that correspond to the sliding of the rod over the dimples or the spring became calmer and

shorter. The reason is that, the increase of the axial force reduces the margin for the tangential sliding either in z or y directions.

The second part of the work was designed for the study of the spring force evolution under irradiation for the 3D model. Initially, the relaxation of the spring force was simulated taking into account each of the three most influent processes in the relaxation of the spring force separately. The results showed that the most influent process for the degradation of the normal force was the irradiation creep. However, when considering all the processes involved in relaxation, results showed that the effect of both creep down and grid growth accelerated the relaxation process. According to the results, the spring would be completely relaxed by 4000 h of the operation cycle, as was expected. In that moment, a gap would open between the fuel rod and the spring. The evolution of this gap is also included as well as a parametrical analysis of the effect of both irradiation creep term and spring stiffness variation.

All the results that have been presented and discussed in this work show that the 2D and 3D model of the fuel rod support implemented in ANSYS predict with a good confidence, the rotational behavior of the fuel rod and the relaxation of the spring force under irradiation. Thus, since the rotational characteristic of the fuel rod within the spacer grid cell determines the mechanical response of the FA to lateral forces and the relaxation of the normal force in the springs implies a decrease of the FA stiffness, this model should be implemented into the complete FA model. This should allow the user to reach more accurate solutions for the bow analysis of the FA.

Cited works

Billerey, A. (2004). *Evolution of fuel rod support under irradiation - Impact on the mechanical behaviour of fuel assemblies*. Villeurbanne, France.

P.Yvon, J. a. (1998). Irradiation Creep and Growth of Guide Thimble Alloys. France.

NTech
Lehrstuhl für
Nukleartechnik

Technische Universität München

Master's Thesis

Ana Alós Díez

Structural Analysis of the Irradiation-Induced Behavior of the Fuel-Rod Support of a PWR Fuel Assembly using the Finite Element Method

Betreuer TUM: Prof. Dr. Rafael Macian-Juan

Betreuer: Dipl.- Ing. Andreas Wanninger

Ausgegeben: 01.11.14

Abgegeben: 15.05.15

Erklärung

Hiermit versichere ich, die vorliegende Arbeit selbstständig und ohne Hilfe Dritter angefertigt zu haben. Gedanken und Zitate, die ich aus fremden Quellen direkt oder indirekt übernommen habe, sind als solche kenntlich gemacht. Diese Arbeit hat in gleicher oder ähnlicher Form noch keiner Prüfungsbehörde vorgelegen und wurde bisher nicht veröffentlicht.

Ich erkläre mich damit einverstanden, dass die Arbeit durch den Lehrstuhl für Nukleartechnik der Öffentlichkeit zugänglich gemacht werden kann.

München, den 15.05.15

Table of contents

Erklärung I
Table of contents I
List of figures III
List of tables V
List of Acronyms VI
Abstract VII
1. General interest of work 1
1.1. Fuel assemblies in a PWR. 2
1.2. Reactor control 3
1.3. Framework of the project: bow analysis. 4
2. Objectives of work 7
2.1. The role of the grid cell springs for fuel assembly stability 7
2.1.1. Rotation of the fuel rod 7
2.1.2. Relaxation of the spring force during the operation of the reactor due to irradiation 13
3. Modeling approaches 19
3.1. APDL 19
3.2. Use of APDL 19
3.3. Description of the ANSYS elements used in the model 20
3.3.1. COMBIN40 20
3.3.2. CONTA178 21
3.3.3. BEAM188 25
4. Description of the model 27
4.1. First part: Nonlinear and hysteretic behavior of the fuel rod support. 27
4.1.1. Fuel rod support: 2D and 3D 27
4.1.2. Application of an axial preload. 34
4.2. Second part: Evolution of the fuel rod support stiffness evolution under irradiation. 35
4.2.1. Implementation of the processes involved on the relaxation of the dimples and the springs. 35

4.2.2. Implementation of the solution 42
4.2.3. Time step selection 44
5. Results 49
5.1. Part 1: Nonlinear and hysteretic behavior of fuel rod support. 49
5.1.1. Fuel-rod support model in 2D 49
5.1.2. Fuel rod support rotation characteristic with 3D model. 54
5.1.3. Rotation characteristic of the fuel rod support with an axial preload. 56
5.2. Part 2: Relaxation of the spring force under irradiation. 60
5.2.1. Model solution 60
5.2.2. Parametrical analysis 64
6. Conclusions 69
Acknowledgements 73
Bibliography 75

List of figures

***Figure 1.1**. PWR plant configuration scheme.....1*

***Figure 1.2.** Fuel assemblies of a PWR.....2*

***Figure 1.3.** Section of a PWR fuel assembly.....3*

***Figure 1.4.** Spacer grid section of a PWR fuel assembly. Example of how fuel rod.....3*

***Figure 1.5.** Representation of how control rods work while controlling the reactor. 4*

***Figure 2.1**. Fuel rod rotation mechanism representation.....7*

Figure 2.2. Fuel rod support representation for 3D model.....8

***Figure 2.3.** Representation of the 2D connection between 9*

***Figure 2.4.** Representation of phases during fuel rod rotation. Gap closed for phases 1a and 1b 9*

***Figure 2.5.** . Phases of rotation evolution of fuel rod support. M=f(θ). 10*

***Figure 2.6**. Representation of ANSYS elements states for the 2D model during rotation.....10*

***Figure 2.7.** Representation of ANSYS elements states for the 2D model during rotation.....11*

***Figure 2.8.** Representation of ANSYS elements states for the 2D model during rotation.....11*

***Figure 2.9**. Representation of ANSYS elements states for the 2D model during rotation.....12*

***Figure 2.10.** Growth representation of a crystal metal. 16*

***Figure 3.1**. COMBIN40 element configuration. 20*

***Figure 3.2.** CONTA178 element geometry.....21*

***Figure 3.3.** Clarification of KEYOPTION(4) of CONTA178.....22*

***Figure 3.4.** Geometry of BEAM188 .....25*

***Figure 4.1.** Implementation of 2D rotation model in ANSYS including node 27*

***Figure 4.2**. Implementation in ANSYS of the 3D rotation model.....28*

***Figure 4.3.** Representation of normal contact for contact elements in ANSYS. 30*

***Figure 4.4**. Representation of tangential contact for contact elements in ANSYS.....30*

***Figure 4.5.** Grid growth as a function of fast neutron fluence for ZIRLO material of spacer grids. 35*

***Figure 4.6.** Grid growth curve obtained from the experimental data in Figure 4.5 .....36*

***Figure 4.7.** Explicit time integration. Forward Euler method. 38*

***Figure 4.8.** Modulus of elasticity of Zircaloy-2 as a function of temperature. 40*

***Figure 4.9.** Schematic application of plastic displacements to the nodes connecting 42*

Figure 4. 10. *Spring relaxation due to irradiation creep. Comparison of different time steps with analytical solution for a simple configuration.* *45*
Figure 4. 11. *Zoom of Figure 4.10.* *45*

Figure 5. 1. *Rotation characteristic for rotation mechanism loading in 2D model* *49*
Figure 5. 2. *Complete loading and unloading of fuel rod rotation for 2D model in both directions about z-axis.* *51*
Figure 5. 3. *Representation of ANSYS elements states for the 2D model during rotation* *52*
Figure 5. 4. *Representation of ANSYS elements states for the 2D model during rotation* *52*
Figure 5. 5. *Representation of ANSYS elements states for the 2D model during rotation* *53*
Figure 5. 6. *Representation of ANSYS elements states for the 2D model during rotation* *53*
Figure 5. 7. *Complete loading and unloading of fuel rod rotation for 3D model in both directions about z-axis.* *54*
Figure 5. 8. *Complete loading and unloading of fuel rod rotation for 3D model in both directions about z and y axes.* *55*
Figure 5. 9. *Loading curve of 3D model with the presence of different axial preloads.* *56*
Figure 5. 10. *Zoom of Figure 5.5.* *57*
Figure 5. 11. *Complete loading and unloading for maximum friction force and without axial force.* *58*
Figure 5. 12. *Plot of burn-up vs time.* *60*
Figure 5. 13. *Relaxation of the spring force due to irradiation creep, spacer grid growth and clad diameter creep down. Three processes separately.* *61*
Figure 5. 14. *Relaxation of the spring force due to irradiation creep, spacer grid growth and clad diameter creep down. All processes acting* *62*
Figure 5. 15. *Relaxation of the spring force and evolution of the gap size.* *63*
Figure 5. 16. *Effect of irradiation creep law effect variation on spring relaxation.* *64*
Figure 5. 17. *Variation of the spring relaxation with several values of the spring normal stiffness.* *65*

List of tables

Table 3. 1. *Normal and tangential behavior of CONTA178 .....24*

Table 4. 1. *Deviations of the results for different simulation times and different time steps 46*

Table 5. 1. *Comparison between model results and analytical ones and the correspondent deviations for the loading curve of the 2D rotation model.....50*

List of Acronyms

APDL	ANSYS Parametric Design Language
FA	Fuel Assembly
FEM	Finite Element Method
FR	Fuel Rod
GT	Guide Tube
IRI	Incomplete Rod Insertion
PWR	Pressurized Water Reactor
SIPA	Stress Induced Preferential Absorption
SIPN	Stress Induced Preferential Nucleation

Abstract

Fuel assemblies within the core of pressurized water reactors are affected by the bow phenomenon, which impacts the performance of the nuclear power plant. Due to the appearance of bending moments, neighboring fuel assemblies can contact leading to spacer grid wear. Furthermore, an excessively distorted FA can induce both safety and operation problems for the reactor. Regarding the safety impact, deformation of the FA can impede the correct insertion of control rods, which is of major importance to control the fission reaction chain. Moreover, FA distortion also induces performance problems increasing refueling times or leading to leaking rods.

However, since bowing involves many different processes, it becomes a challenging issue to predict. For that reason, several computational models have been created over the last years attempting to predict FA bow. The objective of the work which is presented here is to implement a reliable model of the fuel rod to grid connection, which governs the mechanical behavior of the fuel assemblies. Furthermore, the performance of the elements that support the fuel rod within the spacer grid cell is affected by irradiation. In order to study the mechanical behavior of the fuel rod to spacer grid connection, an ANSYS finite element model in both two and three dimensions has been implemented.

This project focuses on the static mechanical aspects concerning the fuel rod support. The work is divided in two different parts: the first one is dedicated to the static rotational behavior of the fuel rod within the grid cell and the second one assesses the relaxation of the spring force during the irradiation of the fuel assemblies. The rotational study of the fuel rod support shows a hysteretic behavior of the static loading and unloading curve caused by the friction elements, which are nonlinear and no conservative. The second study shows the degradation of the spring force under irradiation, which has an exponential evolution. According to results, the supporting springs will be completely relaxed by the end of one operating cycle. The results correspond to what was expected from operational experience but still necessitate thorough validation.

1. General interest of work

Pressurized Water Reactors (PWRs) are currently the most widely used type of nuclear power plants. PWRs obtain the energy released by the fission of a nucleus of Uranium and use this energy to heat water which is used to produce steam that at the end will drive a generator that will provide electrical energy.

A special characteristic of this reactor type is that the water flowing through the first loop is kept at a high pressure, so that boiling inside the reactor is prevented. The reactor core contains the fuel and this is where the nuclear reaction takes place. Once the fission chain is running, the water is heated and used to produce steam within the steam generator. Thermal energy is then transmitted to the secondary loop, where the generated steam enters the turbine. The thermal energy from the steam is transformed into mechanical energy that will drive the generator. Finally, electrical energy is obtained from the generator. The reactor cycle is closed using the condenser. In the condenser, the steam coming from the turbine is condensed with cold water taken from an external source that can be a river, a lake or the sea. At the end, the cooled condensed water is pumped through to the steam generator.

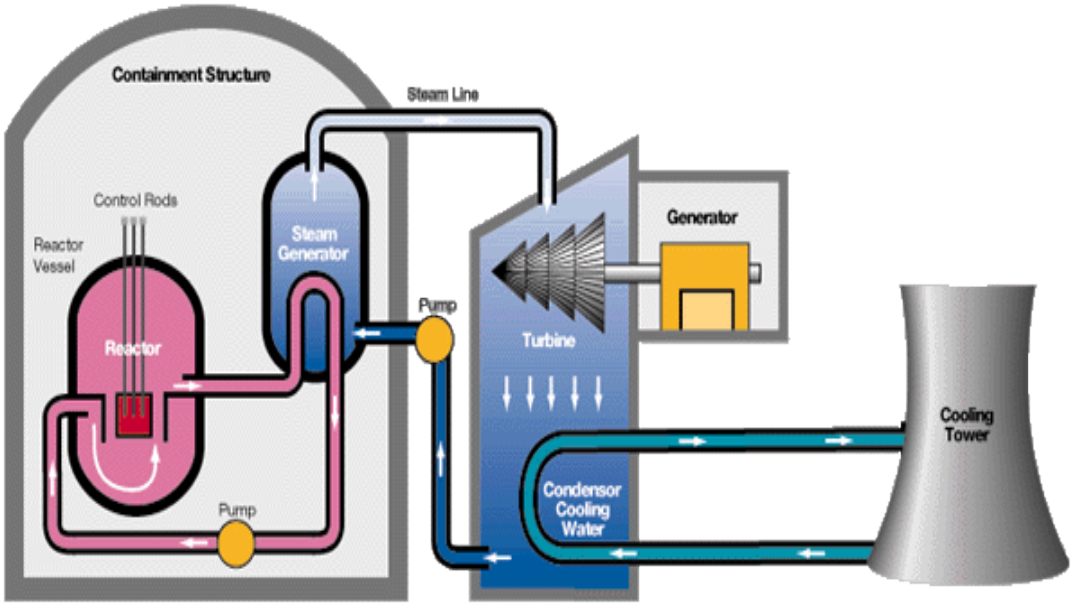

Figure 1. 1. *PWR plant configuration scheme.[1]*

1.1. Fuel assemblies in a PWR.

This work focuses on the reactor core, which is located at the first loop. Nuclear fuel is formed by ceramic pellets of enriched uranium dioxide which are stacked and surrounded by a Zirconium metal alloy cladding. Later on, the fuel rods are gathered in fuel bundles that are otherwise known as fuel assemblies.

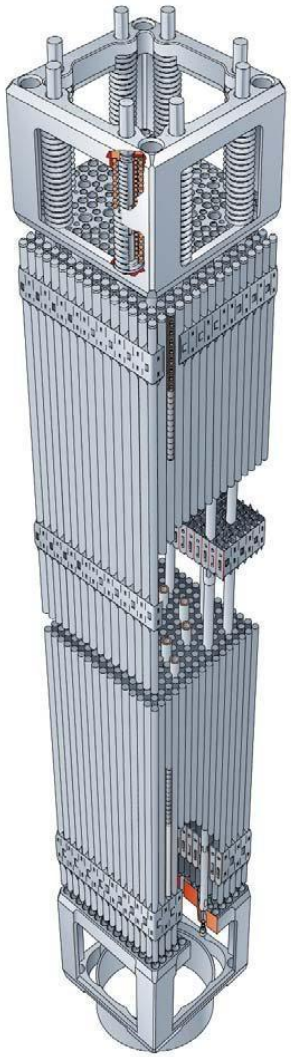

Figure 1. 2. *Fuel assemblies of a PWR [2]*

Within the fuel assembly, rods are placed forming a square matrix usually of, for example, $17x17$, making a total of 289 rods of almost 4 m in length. However, not all of them contain fuel within their structure. A total amount of 264 rods contain fuel, while 24 are intended for the control rod guide thimble and the one left, for the instrumentation thimble. This structure of the rods is ensured by the spacer grids that are placed along the height of the fuel assembly. *Figure 1.3* below visualizes the cross-section of a PWR fuel assembly. [3]

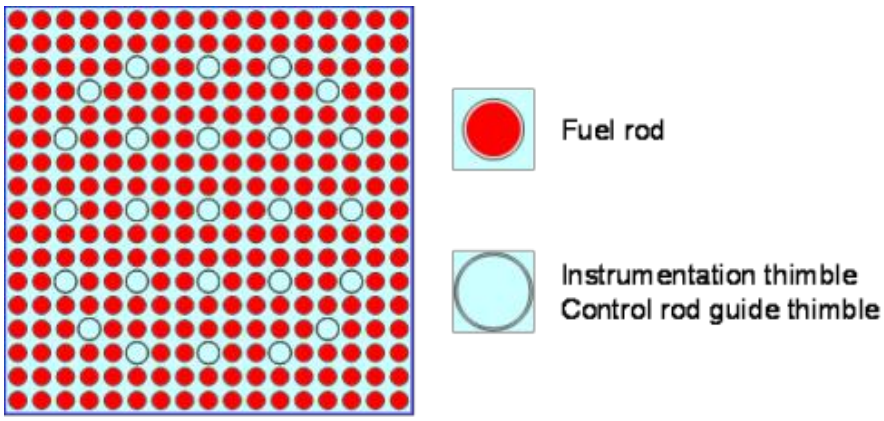

Figure 1. 3. *Section of a PWR fuel assembly [3]*

Spacer grids hold fuel rods in place attempting to reduce fuel rod vibrations. They also contain a series of mixing vanes that enhance heat transfer and coolant mixing. Every spacer grid is divided into squared cells where rods are inserted. In greater detail, fuel rod support is achieved with a combination of springs and dimples placed on the different grid cells in a way that the rod is hold in the middle of the cell. The space between rods, spacer grids and vessel walls is filled with a special coolant. [4]

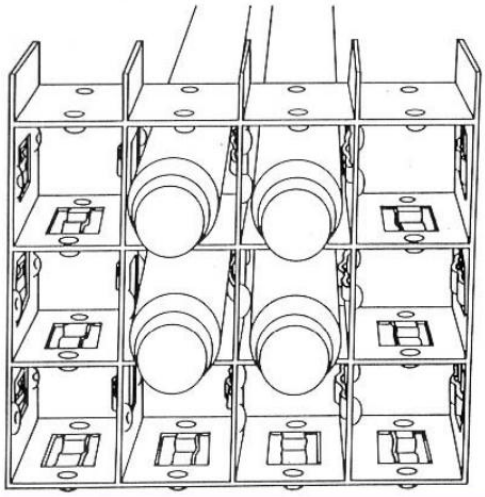

Figure 1. 4. *Spacer grid section of a PWR fuel assembly. Example of how fuel rod supports look like. [4]*

1.2. Reactor control

Reactor control is achieved using two different methods. On one hand, first loop coolant is mixed with boric acid to increase the moderator capability to absorb neutrons and thus, slow down the chain reaction. On the other hand, control rods are moved up or down the

control rod guide thimble, depending on the desired result. Hence, if the objective is to shut down the reactor, the insertion of control rods will interrupt the chain reaction. On the contrary, control rods are withdrawn for start up the reactor. Therefore, control rods attempt for the reactor reactivity control that can be positive, negative or one. [5]

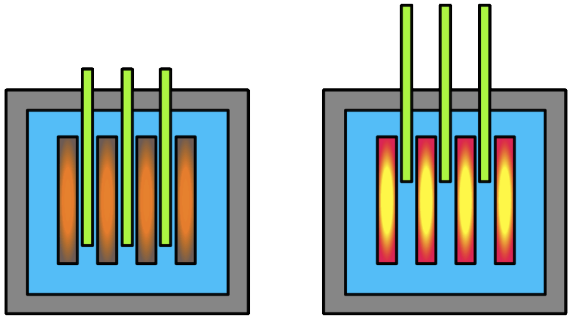

Figure 1. 5. *Representation of how control rods work while controlling the reactor.[5]*

Figure 1.5. shown above exemplifies the role of control rods in regulating the power in the core. In the image on the left, control rods (green color) are completely inserted in the core as is done when the reactor is shut down. Then, the absorption of neutrons increases, putting the reactor in a subcritical state and hence, stopping the fission chain. On the contrary, in the image on the right, control rods are removed from the core, reducing the neutron absorption and enhancing the fission chain, which results in a supercritical reactor state.

The capability to absorb neutrons determines the control rod material, which is measured by σ_a, which is also its absorption cross section. Consequently, materials with a high absorption rate will be preferred.

1.3. Framework of the project: bow analysis.

Bow analysis is a very concerning issue for nuclear engineering because of its important impact on the performance of the power plant. During reactor operation, fuel assemblies are affected by various processes which are governed by a wide quantity of factors. Power density gradients that are present generate different growth rates of fuel rods as well as different elongations due to thermal processes. As a consequence of the variety of axial forces within a fuel assembly, bending moments can appear. Furthermore the relaxation of the springs supporting the fuel rod within a spacer grid cell has an important effect on the bowing of the FA.

Occurrence of this bowing phenomenon can have a big impact on PWR operation. After the FA has bent, contact between adjacent assemblies can appear and it can result in spacer grid wear. Consequences of bowing cause both operational and safety hazards. On

one hand, bowing affects the correct insertion of control rods, which is fundamental for controlling the reactor. When this occurs, both incomplete rod insertion and an increase of the time invested in dropping the control rods can be observed. Due to the deformation of the fuel assemblies water gaps are formed, resulting in a perturbation of power distribution and consequently the decrease of thermal margins. Furthermore, friction forces between fuel assemblies increase refueling times.

However, the variety of physical processes involved in FA bowing (structural, thermal materials, hydraulic and neutronic) and all reactor elements subjected to deformation makes it a difficult issue to predict, since it becomes a relatively complex process. In addition, the problem must be studied simultaneously on a small scale (fuel rod-to-grid connection) as well as on a larger scale (taking into account the entire core with all loads). In order to simplify the problem, the different effects are considered as additive processes.

The objectives of the bow analysis model are to implement a reliable tool that could predict FA bow, investigate the parameters which have the strongest effect on the bowing phenomenon, and also provide assessment for possible new FA design modifications. [6] [7][8].

2. Objectives of work

2.1. The role of the grid cell springs for fuel assembly stability

The mechanical behavior of the fuel rod support influences, amongst others, how the fuel assemblies will behave under irradiation. Therefore, it is essential to have a precise knowledge of the fuel rod to spacer grid connection in order to predict and prevent possible operation and safety problems induced by the mechanical behavior of this connection. The present study shall consider the static mechanical aspects which can be split into two parts: the static rotational behavior of the fuel rod in the grid cell and the evolution of the spring force under irradiation.

The rotational behavior of the fuel rod determines the mechanical response of the FA to lateral forces, since the presence of the fuel rods gives additional stiffness to the FA skeleton. The degradation of grid cell spring force under irradiation hence implies a stiffness decrease of the FA which should be accounted for bow analysis. Additionally, the behavior of the fuel rod support has an influence on the vibration properties of the fuel rod, which are, however, not a part of the present study.

2.1.1. Rotation of the fuel rod

The support of the fuel rod is achieved with a combination of four dimples and two springs placed in two perpendicular planes. Thus, the fuel rod is supported on a three dimensional level.

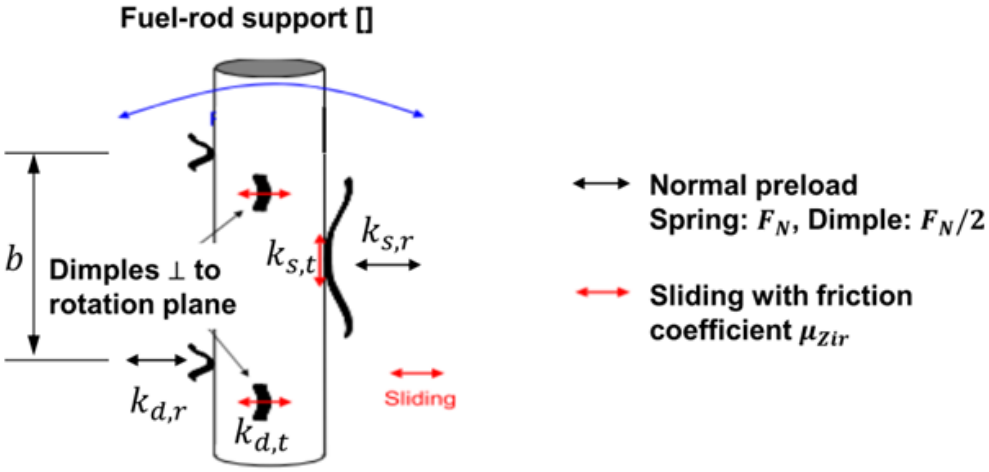

Figure 2. 1. *Fuel rod rotation mechanism representation[9]*

Figure 2.1. depicts how the fuel rod support looks with the dimples and springs. It also includes the sliding directions with their corresponding stiffness, the normal preloads and the rotational direction. The spring is initially preloaded with a normal force F_N and meeting the static equilibrium, the normal preload for the dimples will be half of the spring force for each one, which is $F_N/2$. As the fuel rod rotation increases, it can shift from the contact elements and if the rotation continues, a gap between the spacer grid dimple and the rod may appear. [9]

In three dimensions, the complete support mechanism looks schematically like this:

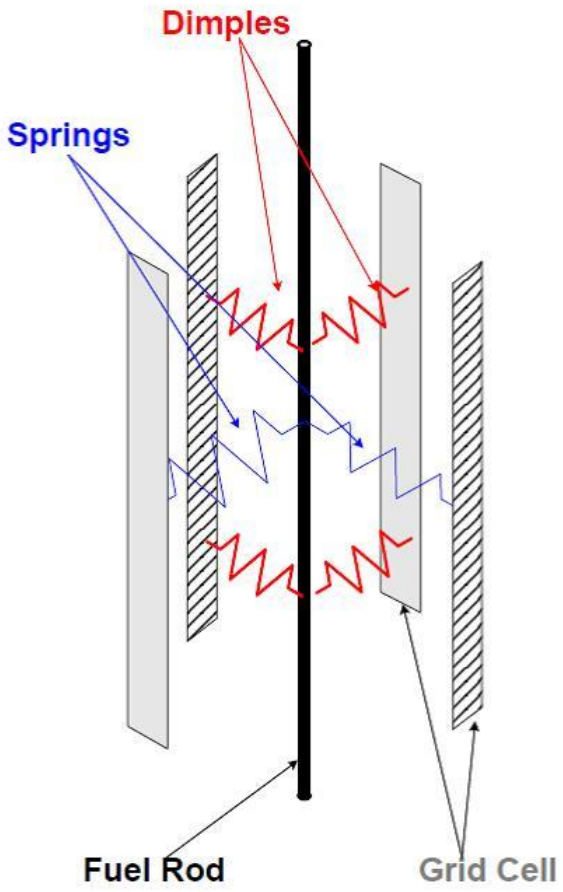

Figure 2. 2. *Fuel rod support representation for 3D model.[9]*

In the case of 3D, there are two planes of rotation, which are both perpendicular. Each plane contains the same elements and is equal to the one presented for the 2D model (see *Figure 2.2*).

The figure below shows a schematic model of one of the two planes containing the fuel rod, two dimples and one spring. It also exemplifies the rotation of the rod about the axis that is normal to the rotation plane.

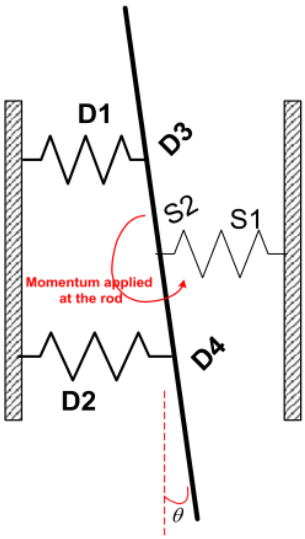

Figure 2. 3. *Representation of the 2D connection between fuel rod and spacer grid while rotation.[9]*

In *Figure 2.3*. $D1, D2, D3$ and $D4$ stand for the dimples and $S1, S2$ for the springs. Additionally, the center beam counts for the fuel rod and the external fixed walls for the spacer grids of the fuel assemblies. As the rotation increases, the fuel rod will slide from the dimples and eventually, a gap between one of the dimples and the rod may open. Regarding the existence of the gap, the rotation process has two main states: contact or opening gap of the rod-to-grid connection.

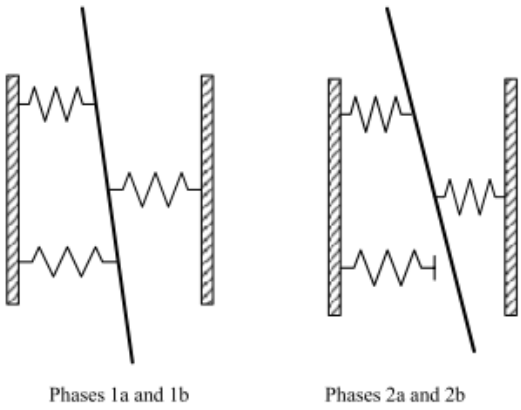

Figure 2. 4. *Representation of phases during fuel rod rotation. Gap closed for phases 1a and 1b on the left) and open for phases 2a and 2b (on the right) [9]*

From previous studies, it is known that the evolution of the fuel rod rotation is divided into four phases, as shown in *Figure 2.5*. This rotational behavior is obtained by solving

the static equilibrium of all the forces and moments involved in one of the perpendicular planes which contains two dimples and one spring of the fuel rod support system.

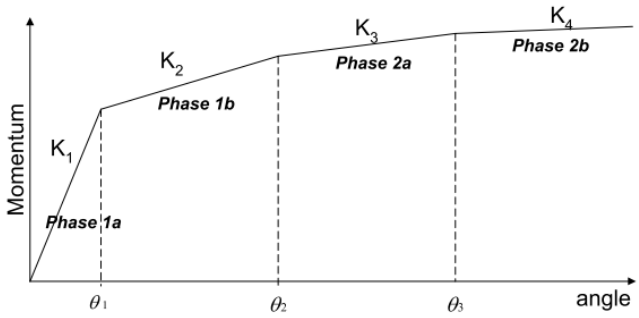

Figure 2. 5. . *Phases of rotation evolution of fuel rod support. M=f(θ).[9]*

During the four phases, the elements go through various states that are specified as follows [9]:

- **Phase 1a**: At the beginning of the rotation both dimples start loading, while the spring remains at rest due to the location of the rotation center that stays at the same point. The normal force of the dimple that is being compressed increases and the one of the dimple being decompressed decreases in the same proportion. The two dimples and the spring perpendicular to the rotation plane are in sticking contact with the fuel rod because the tangential forces do not exceed the maximum force for sliding.

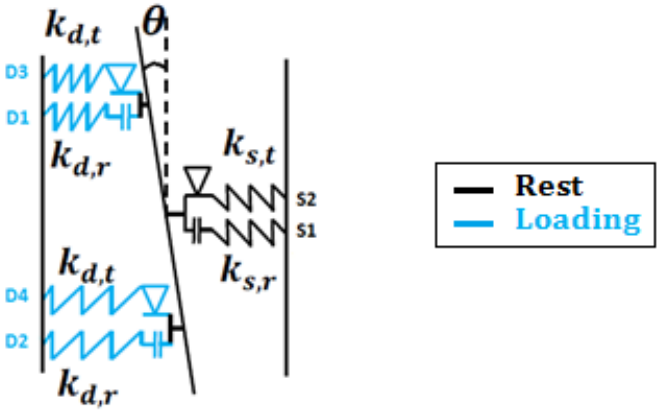

Figure 2. 6*. Representation of ANSYS elements states for the 2D model during rotation of the fuel rod. Phase 1a [10]*

- **Phase 1b**: As the moment increases, the fuel rod stays in contact with both dimples and the spring but now, as the tangential forces reach the maximum sliding force, it slides over the dimples in a plane perpendicular to the rotational one. The dimples placed on the rotational plane are still loading and the spring is at rest because the rotation point is still central.

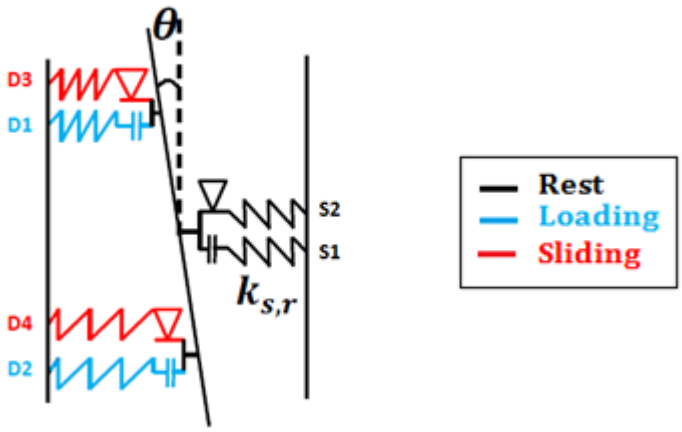

Figure 2. 7. *Representation of ANSYS elements states for the 2D model during rotation of the fuel rod. Phase 1b [10]*

- **Phase 2a**: At one time, the dimple which is unloaded is totally decompressed and the fuel rod shifts away from it while the other dimple is still loading. The symmetry is broken and the spring is loaded. The perpendicular spring stays in sticking condition.

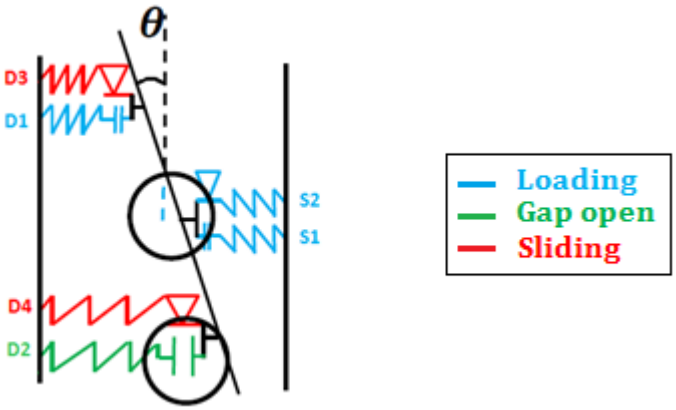

Figure 2. 8. *Representation of ANSYS elements states for the 2D model during rotation of the fuel rod. Phase 2a [10]*

- **Phase 2b**: Finally, the fuel rod slides over the spring in a plane which is perpendicular to the rotational plane. The gap between the fuel rod and one of the dimples remains open and the perpendicular dimples are in sliding contact with the fuel rod.

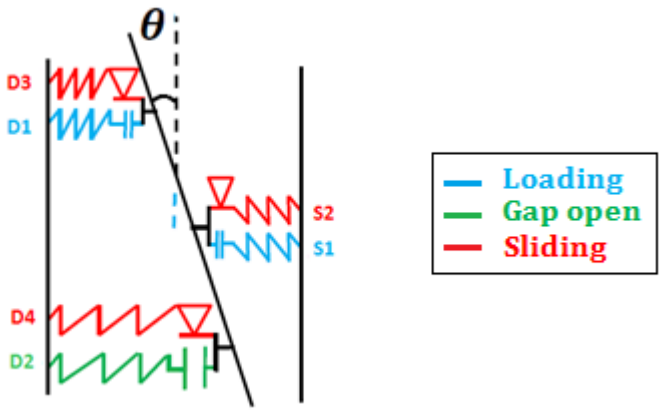

***Figure 2. 9**. Representation of ANSYS elements states for the 2D model during rotation of the fuel rod. Phase 2b [10]*

The analytical values of the rotation angles and the moments that correspond to the thresholds between the four different phases are obtained by solving the static equilibrium of forces and moments and applying the limiting conditions for changing the phase: [10]

The initial conditions before rotation starts are:

$$\theta_0 = 0 \qquad \textit{Equation 2. 1}$$

$$M_0 = 0 \qquad \textit{Equation 2. 2}$$

Phase 1a-1b

$$\Delta\theta_1 = \frac{\mu \cdot F_N}{b \cdot k_{d,t}} \qquad \textit{Equation 2. 3}$$

$$\theta_1 = \theta_0 + \Delta\theta_1 \qquad \textit{Equation 2. 4}$$

$$M_1 = M_0 + k_{\theta_1} \cdot \theta_1 = k_d \frac{b^2}{2} \cdot \theta_1 \qquad \textit{Equation 2. 5}$$

Phase 1b-2a

$$\Delta\theta_2 = \frac{F_N(1 - \mu \frac{k_{d,r}}{k_{d,t}})}{b \cdot k_{d,r}} \qquad \textit{Equation 2. 6}$$

$$\theta_2 = \theta_1 + \Delta\theta_2 \qquad \textit{Equation 2. 7}$$

$$M_2 = M_1 + k_{\theta_2} \cdot \Delta\theta_2 = M_1 + k_{d,r}\frac{b^2}{2} \cdot \Delta\theta_2 \qquad \textit{Equation 2. 8}$$

Phase 2a-2b:

$$\Delta\theta_3 = \mu F_N \cdot \frac{k_s + k_{d,r}}{\frac{b}{2} \cdot k_{d,r}k_{st}} \qquad \textit{Equation 2. 9}$$

$$\theta_3 = \theta_2 + \Delta\theta_3 \qquad \textit{Equation 2. 10}$$

$$M_3 = M_2 + k_{\theta_3} \cdot \Delta\theta_3 = M_2 + \frac{b^2}{4} \cdot \frac{k_s k_{d,r}}{k_s + k_{d,r}} \cdot \Delta\theta_3 \qquad \textit{Equation 2. 11}$$

End of the loading:

$$\Delta\theta_4 = 2\theta_3 \qquad \textit{Equation 2. 12}$$

$$\theta_4 = \theta_3 + \Delta\theta_4 \qquad \textit{Equation 2. 13}$$

$$M_4 = M_3 + k_{\theta_4} \cdot \Delta\theta_4 = M_2 + \frac{b^2}{4} \cdot \frac{k_{s,r} k_{d,r}}{k_{s,r} + k_{d,r}} \cdot \Delta\theta_4 \qquad \textit{Equation 2. 14}$$

2.1.2. Relaxation of the spring force during the operation of the reactor due to irradiation.

This spring force relaxation appears as a consequence of the occurrence of three main processes while the reactor fuel burns. This section further investigates these processes with a short explanation of their origins and the consequences on the fuel rod behavior.

❖ Creep-down of the clad diameter

The fuel rods that are organized into fuel assemblies contain stacked pellets of uranium dioxide. This column of pellets is thinner than the cladding inner diameter, so there is a gap between the pellets and the clad wall. This gap is left because, as the fission reaction chain evolves, fission gases are released and then, they fill the surrounding space around the pellets.

Furthermore, the fuel rod is surrounded by the coolant that has a pressure of around $155\ bar$. Before the fission reaction starts, the pressure inside the fuel rod clad is lower than the coolant pressure, since the gap between clad and pellet is filled with He gas at a pressure of $20\ bar$. This difference of pressure creates a force on the clad surface directed towards the low pressure volume, generally inward stresses. Under influence of these stresses, creep processes lead to a plastic decrease of the cladding diameter under irradiation, which is known as fuel rod creep-down. As the fission process continues, fission gases are released and then the pressure inside the clad increases, decreasing gradually the pressure difference. Additionally, when the internal pressure of the released gases exceeds the external pressure which remains constant, the entire distribution of forces reverses and consequently, the clad diameter starts to increase again.

- Irradiation creep and growth

Before explaining these two processes separately, and in order of have a better understanding of how the clad material behaves under irradiation, a first overview about the creep phenomenon is incorporated here.

When a metal is submitted to a constant load under high temperatures, it suffers creep, which is a deformation of the metal depending on the temperature. Creep is translated into a metal elongation that can be expressed as the correspondent strain and can either be defined as the nominal (ε) or the true strain (ε_T).

Being:

$$\varepsilon = \int_{l_0}^{l} \frac{dl}{l_0} = \frac{l - l_0}{l_0} \qquad \textit{Equation 2.15}$$

$$\varepsilon_T = \int_{l_0}^{l} \frac{dl}{l} = \ln \frac{l}{l_0} = \ln(1 + \varepsilon) \qquad \textit{Equation 2.16}$$

The difference between the nominal and the true strain relation with their correspondent stresses is that the nominal strain relates to the nominal stress through the initial cross section, while the true strain relates through the instantaneous cross section. Also, creep is referred to the plastic component of the strain that is as well time-dependent.

From the metal crystal lattice level, creep occurs because the irradiation of a metal creates the appearance of vacancies and point defects. At that point, the vacancies and dislocations move through the lattice by diffusion. Thus, creep depends on the probability of vacancies formation and also on the movement of vacancies and point defects. In addition, creep also depends on the stress. [11]

❖ Irradiation creep

The creep component related to radiation is assumed to be independent on the temperature. The reason is that the formation of defects and vacancies is not originated by thermal processes, but by the atomic displacement as a consequence of the differences of energy along the lattice. Nevertheless, irradiation creep depends on both the stress and the neutron flux. The effect of irradiation is that it accelerates the formation of vacancies and dislocations on the crystal lattice and thus, it enhances the creep rate. However, it is not the only aspect that has to be considered. The existing stress and the motion of point defects changing the microstructure of the crystal should also be analyzed.

There are two mechanisms that explain the irradiation creep in metals:

- Stress Induced Preferential Absorption (SIPA): atoms from planes parallel to the applied stress are accumulated on planes perpendicular to the stress.
- Stress Induced Preferential Nucleation (SIPN): nucleation of interstitial loops is more likely to happen on planes perpendicular to the normal applied stress.

Point defects produced by irradiation exposure tend to change their location in a way that the energy of the system will be reduced. With this purpose they usually move to dislocations and grain boundaries.

In general, the expression by which reactor creep is governed is:

$$\dot{\varepsilon} = A\sigma^n \phi^p G_d e^{-(\frac{Q}{RT})} \ [f(t) or\ g(\varepsilon)] \qquad \textit{Equation 2.17}$$

A Area of slip plane or dislocation loop

σ Stress

ϕ Neutron flux

Q Activation energy for the rate limiting process

n, p Stress and flux exponent

G_d Factor of growth anisotropy

The value of n for low stresses ($< 1/3\sigma_y$), being σ_y the stress in y-direction, and temperatures around 300℃ is equal to 1 for Zr alloys and for low fluxes, p takes values from 0.25 up to 0.85. The creep rate expression can be a function of time ($f(t)$) for the case of time hardening or a function of strain ($g(\varepsilon)$) for the case of strain hardening. Besides that, the term $e^{-(\frac{Q}{RT})}$ counts for the probability of vacancy formation and vacancy or dislocation motion, which is proportional to this factor [11].

❖ Grid growth

Under irradiation, materials of the core components suffer the appearance of vacancies and interstitials. Without stress, point defects that appear in crystal lattices of anisotropic materials, such as Zirconium, will move preferably to dislocations that are located on prism planes and to grain boundaries parallel to prism planes. On the other hand, vacancies tend to move to basal planes or to grain boundaries parallel to those planes. Finally, the result is that the metal elongates in one direction and compresses in the other and that is what is known as irradiation growth.

The Zirconium alloy of which the spacer grids in the active region of the core are made of is affected by two processes that at the end will induce material growth. In addition to the fast neutron fluence growth, the thin material makes the spacer grids prone to also undergo growth from the hydrogen pick-up originated by corrosion. Thus, in the absence of stress, the crystal form of the Zircaloy is distorted while conserving its original volume (see *Figure 2.10*). [11] [12]

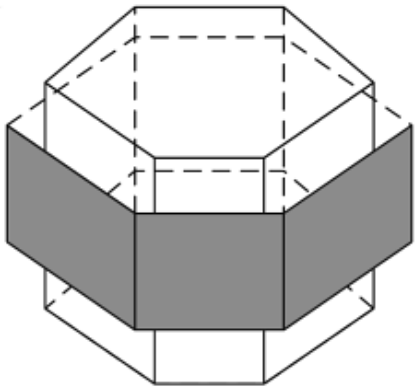

Figure 2. 10. *Growth representation of a crystal metal*.

In conclusion, the combination of all these processes that take place during the irradiation of the fuel assemblies can lead to both safety and operation problems. The distortion of the fuel assemblies creates problems related with the insertion of the control rods that are of major importance to control the chain fission reaction. . Furthermore, the wear induced by fuel rod vibration can end up in leaking rods that will provoke operation problems on the nuclear reactor plant. That is why the study and understanding of the mechanical behavior of the fuel rod support during operation is such an important issue. Moreover, it was said that the temperature is not that influent on irradiation creep, so for the study of these processes rather a mid-grid cell with medium temperatures, low stress and high neutron flux will be analyzed.

3. Modeling approaches

3.1. APDL

APDL is the acronym of ANSYS Parametric Design Language, which is a powerful feature of ANSYS that can be used to type a model in terms of parameters and also allows the automation of common tasks. By parameterizing the model, the user can easily obtain precise information about the influence that the different parameters involved may have in the final solution. Moreover, since the user has complete control over the model, any parameter value can be simply modified by only changing the parameter definition [13] [14].

Some of the advantages of this parametric language are the use of:

- Repetition of commands.
- Branching (if-then-else) and do-loops.
- Operations with scalars, vector and matrix.
- Macros: a file composed of ANSYS commands that can be executed from the model as a normal command.

3.2. Use of APDL

The scripting process consists of three main parts:

- Preprocessing: it contains all the geometric specifications, the properties of the element materials and also the finite element model generation. Concretely, the main tasks that are accomplished in this part are:
  - Material properties definition.
  - Element set-up with the definition of real constants if it was required by the element type.
  - Model geometry specification.
  - Mesh generation.
  - Model constraints specification.
- Solution: is the part where the loads are applied and where the algorithm that let the user get the solution of the finite element model is performed.
- Post processing: in this part the results of the FEM can be reviewed. The results can be displayed by:
  - Plots.
  - Vector displays.
  - Files containing vector or tabular information about the displacements, stresses, forces, node locations, etc.

3.3. Description of the ANSYS elements used in the model

The aim of this thesis is to create a finite element model in two and three dimensions of the fuel rod support within a grid cell of the PWR fuel assemblies. Then, contact elements are needed to model the contact between the fuel rod, the grid cell, and a beam element for the fuel rod. More information about these ANSYS elements used in the FEM is given hereafter.

3.3.1. COMBIN40

The COMBIN40 is a status dependent element, so its behavior is nonlinear. The element consists of a parallel combination of a spring-slider and damper with a gap which is coupled in series (see *Figure 3.1*). This combination element has only one degree of freedom at each node which can either be: nodal translation or rotation. For the model presented here the damping capability and the slider are removed.

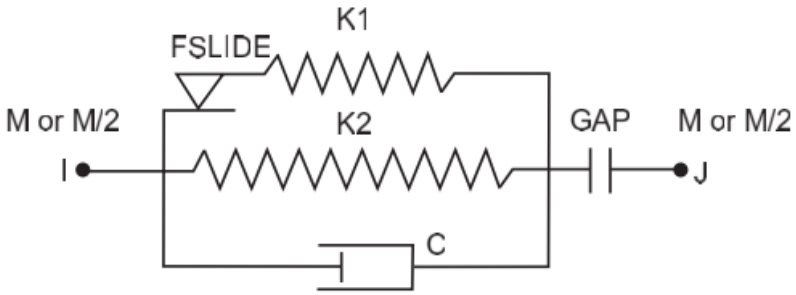

Figure 3. 1. COMBIN40 element configuration.

The values of the parameters are assigned with the real constants definition and cannot be changed from the initial values. If either the spring constants or the damping coefficient are zero, these capabilities will be removed from the element. In this case, since COMBIN40 is used to represent the normal contact, the only parameters that are specified are $K2$ and the gap size GAP. The rest of the parameters are equal to zero.

For the GAP capability, three different options are available. A negative value of the GAP creates an initial interference that will correspond to that quantity. If $GAP = 0$, the gap capability is removed and if the value is positive, an initial gap of this amount exists. When using this element for the model the state of the gap provides information about whether the fuel rod is in contact with the spacer grid or not.

The input data is determined by setting the values of two different parameters: the KEYOPTIONS and the real constants. With the first ones, the gap behavior, the degree of freedom, the element output, and the mass distribution are selected, while the real constants will specify the values of $k_1, C, M, GAP, FSLIDE$ and k_2.

Regarding the solution, the element output is given in two different ways:

- The degree of freedom of the nodes is included in the total nodal solution.
- Other useful information is also provided by the program:

    - $STR = U(J) - U(I) + GAP - SLIDE$ is the displacement of the spring at the end of the last sub step. Where $SLIDE$ is the total sliding at the end of the substep referred to the initial position, and $U(J)$ and $U(I)$ the initial locations of nodes J and I respectively.

    - For the model validation the output value $STAT$ was useful, whose value provides information about the state of the contact at the end of each sub step. For instance, the contact can be open ($STAT = 3$), closed without sliding ($STAT = 1$) or closed but sliding in either a positive ($STAT = 2$) or negative ($STAT = -2$) direction.

3.3.2. CONTA178

This element represents contact and sliding between two nodes of two different elements, no matter which type of elements they are. It consists of two nodes with three degrees of freedom at each node, which are the displacements along the three axes UX, UY and UZ respectively. CONTA178 can be used not only in 3D models, but also in 2D ones by constraining the UZ degree of freedom. The element can support both compression in the contact normal direction and Coulomb friction in the tangential one. Initially either a gap or a normal preload can be specified.

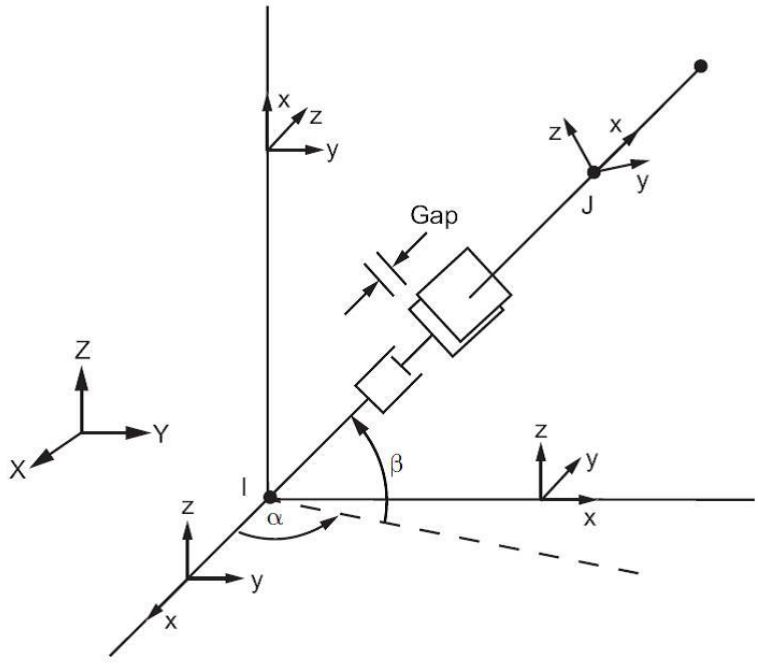

Figure 3. 2. *CONTA178 element geometry.*

For the definition of the element the contact normal and the node locations have to be known. Moreover, an initial preload or gap is defined, as well as the initial status of the element. Besides that, the interference is supposed to be parallel to the plane YZ of the element coordinate system.

Similarly to COMBIN40, CONTA178 is completely defined by setting the values of the KEYOPTIONS and the real constants.

With the KEYOPTIONS, the unidirectional gap type for this case and the algorithm used for the resolution of the contact problem can be selected. Furthermore, the bases for the gap size and for the contact normal are chosen. Thus, the gap size can be based on the value of the real contact called GAP and node positions, or only on the real constant. The figure below exemplifies these two possibilities for the gap size that are selected by fixing the value of KEYOPT(4).

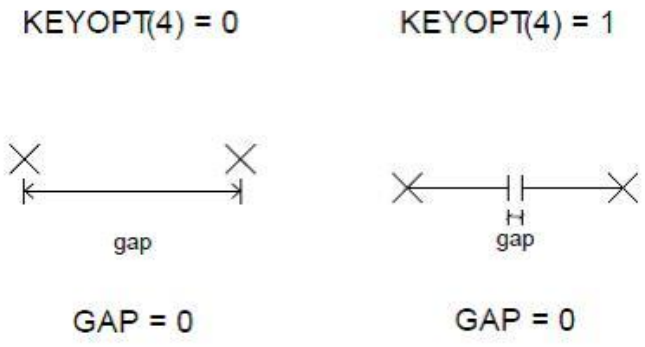

Figure 3. 3. *Clarification of KEYOPTION(4) of CONTA178*

The definition of the contact normal is especially important in a contact problem. If KEYOPT(5)=0 and the real constants NX=NY=NZ=0, the contact normal direction will be calculated based on the initial positions of the nodes. Then, the gap will open as node J moves in a positive direction along the x-element axis. Nevertheless, as the model has an initial interference condition in which the geometry of the elements overlaps, the normal direction must be specified.

$KEYOPT(2) = 1$ determines the contact algorithm, which is the Pure Penalty Method. While selecting this method for the calculations, both normal and tangential values FKN and FKS are required by the program.

For the implementation of the Pure Penalty Method, ANSYS uses the Newton-Raphson load vector, which is:

$$\{F_l^{nr}\} = \begin{Bmatrix} F_n \\ F_{sy} \\ F_{sz} \\ -F_n \\ -F_{sy} \\ -F_{sz} \end{Bmatrix} \qquad \textit{Equation 3. 1}$$

Where:

$F_n =$ Normal contact force

$$F_n = \begin{cases} 0 & if\ u_n > 0 \\ k_n u_n & if\ u_n \leq 0 \end{cases} \qquad \textit{Equation 3. 2}$$

Being k_n the normal contact stiffness (FKN) and u_n the size of the contact gap.

$F_{sy} =$ Tangential contact force in the Y direction.

$$F_{sy} = \begin{cases} k_s u_y & if\ \sqrt{F_{sy}^2 + F_{sz}^2} - \mu F_n < 0 \quad Sticking\ contact \\ \mu k_n u_n & if\ \sqrt{F_{sy}^2 + F_{sz}^2} - \mu F_n = 0 \quad Sliding\ contact \end{cases} \qquad \textit{Equation 3. 3}$$

With:

$k_s =$ Tangential contact stiffness (FKS)

$u_y =$ Contact slip distance in y-direction

$\mu =$ Friction coefficient (MU)

And,

$F_{sz} =$ Tangential contact force in the z-direction.

The most basic and important real constant that have to be defined for the presented model are:

$FKN =$ Normal stiffness

$GAP =$ Gap size

$START =$ Initial contact status

$FKS =$ Tangential stiffness

NX, NY and $NZ =$ Gap normal component that can be either the x,y or z directions.

The $START$ parameter determines the status of the contact at the beginning of the first sub step. Thus, if $= 0$, the initial condition is calculated with the value of the GAP real constant or with the specification of the fourth KEYOPTION. The gap can also be initially open, if $START = 1$ or closed and sliding if $START = 2$. Moreover, a value of $START = 3$ determines an initial closed gap either sticking (if $\mu \neq 0$) or sliding (if $\mu = 0$). The status of the contact during the different sub steps of the simulation depends on both the normal and tangential forces. Regarding the normal force, the gap will remain closed with a negative value of F_N, that means that the contact element is compressed. The limiting tangential force above which sliding occurs is $\mu \cdot |F_N|$, being μ the friction factor and the only structural material property used for the friction characteristic of the model.
The output of CONTA178 is given in two different ways:

- The displacements of the nodes are included in the total nodal solution.
- The state of the contact at the end of the sub step is also available.

Normal force	**GAP**	**Tangential force**	**Tangential contact**	**STAT**
$\boldsymbol{F_N} < 0$	Closed	$\boldsymbol{F_S} < \mu \cdot \lvert \boldsymbol{F_N} \rvert$	Sticking	3
		$\boldsymbol{F_S} < \mu \cdot \lvert \boldsymbol{F_N} \rvert$	Sliding	2
$\boldsymbol{F_N} = \boldsymbol{0}$	Open	$\boldsymbol{F_S} = \boldsymbol{0}$	No contact	1

Table 3.1. *Normal and tangential behavior of CONTA178*

3.3.3. BEAM188

BEAM188 is a 3D linear, quadratic or cubic beam element connecting two nodes with six degrees of freedom at each node that can be either translations along the three axes and rotations around the x, y and z directions.

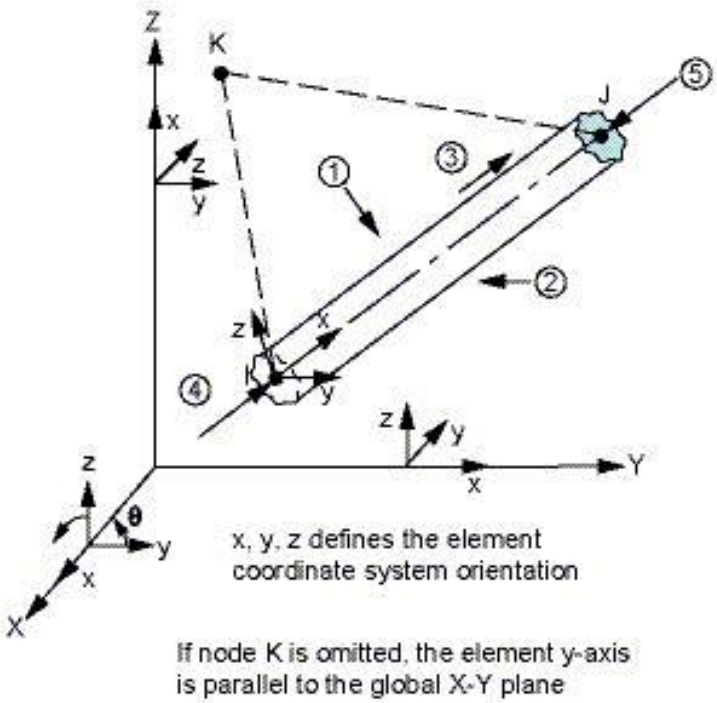

Figure 3. 4. *Geometry of BEAM188.[16]*

The element is defined by nodes I and J and the orientation of the beam is fixed by the third node K. However, it is not mandatory to define this third node K.

It is especially appropriate for modeling slim to moderately thick beams. The element supports nonlinear material models, as well as, elasticity, plasticity and creep. Besides that, the cross-sections are not distorted and remain on plane after deformation. In the model, BEAM188 is used to model the fuel rod beam.

Although BEAM188 is also defined by using the corresponding KEYOPTIONS, the beam cross-section characteristics are set apart and related to the element by an ID number.

The shape function that is used along the length is a quadratic one. The use of this function has two limitations:

- The initial geometry of the element is treated as straight.
- In the internal nodes there are neither initial nor boundary, nor loading conditions. The reason is that these nodes are internal and thus, inaccessible.

In terms of load conditions, the forces are applied at the nodes and pressure loads can also be inputs if applied as surface loads. If the input pressure was lateral, it would be treated as force per unit length. Besides that, temperature can be input at the ends of the element. Axial forces can induce bending of the beam if it is the case where the centroidal axis was not collinear with the x-axis of the element.

4. Description of the model

This section includes the presentation of the two parts in which this work is divided. The first part describes the most relevant information that is required to implement the model used to study the rotational evolution of the fuel rod without counting for irradiation. It includes both a 2D and a 3D model. The second part contains the explanation of the model implemented to study the evolution of the spring force as the reactor operation time increases. Both parts describe how the preprocessing and post processing parts were performed.

4.1. First part: Nonlinear and hysteretic behavior of the fuel rod support.

4.1.1. Fuel rod support: 2D and 3D

Based on the rotation model of the fuel rod presented in [10], the 2D model of the fuel rod support has been implemented in order to study its rotation mechanisms by solving the static equilibrium.

The fuel rod support configuration of the ANSYS 2D model, including the nodes, the elements used and the geometric dimensions is shown in the following figure:

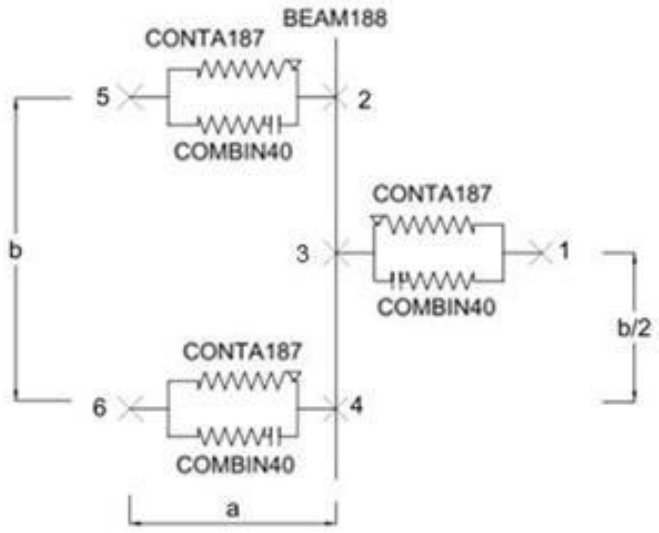

Figure 4. 1. *Implementation of 2D rotation model in ANSYS including node locations and element types.*

The ANSYS configuration that was implemented to model the fuel rod support within a grid cell of the fuel assembly is shown in the figure above. The contact elements represent

the normal and tangential contact of the dimples and the spring supporting the fuel rod, which is modeled with a beam between nodes 2-3 and 3-4. Apart from that, the external nodes are constrained in a way that they are fixed so that they represent the grids.

For the 3D model the total configuration consists of two planes equal to the one described for the 2D model but placed perpendicular to each other. Hence, the complete model will consist of four dimples and two springs placed into two perpendicular planes with two dimples and one spring in each of these planes. As it is was shown in *Figure 2.2*, the 3D model has nine nodes, so the three new nodes that correspond to the perpendicular plane XZ must be added to the node definition of the model (see *Figure 4.2*).

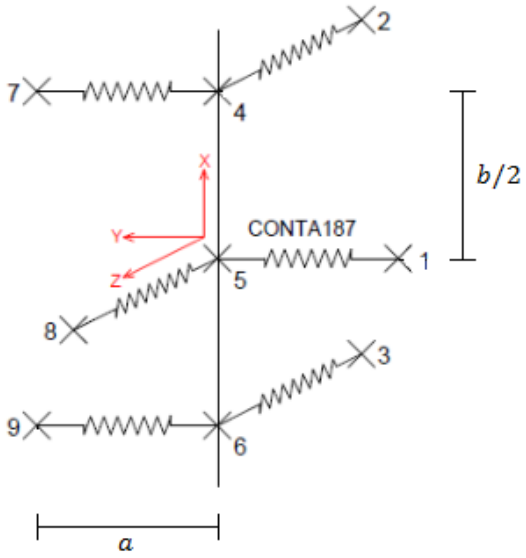

Figure 4. 2. *Implementation in ANSYS of the 3D rotation model.*

Only BEAM188 and CONTA178 elements

In order to define the node locations, the dimensions of the fuel rod and the pitch have to be known. The fuel rod has an outer diameter of 10.75 mm and the pitch of the grid cell is of 14.3 mm [18]. Then, the distance between the fuel rod outer surface and the grid cell is of 1.775 mm on each side, which is actually the compressed length of the spring before irradiation and without any additional load. With this data and the axial distance between the dimples which is assumed to be 20 mm the following parameters are used:

$a = 0.001775\ m$

$b = 0.020\ m$

$pitch = 0.0143\ m$

4.1.1.1. Definition of the elements used in ANSYS to implement the model.

- **FUEL RODS**

The beam element that is used here to implement a single rod, which is the object of study, is the **BEAM188**. This element is a beam in 3D that connects two nodes. In the model, the beam element is used twice; one to connect nodes 2 and 3 and the other one to connect nodes 3 and 4. The beam will behave as a single element with the two different parts perfectly coupled. The fuel rod beam element is used for both the 2D and 3D models.

For the definition of the beam element, the first characteristic to be selected is the section type. In this case the $ASEC$ section, which is an arbitrary section, is chosen. This *ASEC* section requires the user to provide the cross-section inertia properties instead of the geometry data.

The relevant cross-sectional parameters provided by the user to completely define the beam section are:

$A =$ Section area

$$A = \pi(R_{out}^2 - R_{inn}^2) \qquad \textit{Equation 4. 1}$$

Where R_{out} is the fuel rod outer radius and R_{inn} the fuel rod inner one.

$I_{yy} =$ Moment of inertia about the y axis

$$I_{yy} = \frac{\pi}{4}(R_{out}^4 - R_{inn}^4) \qquad \textit{Equation 4. 2}$$

$I_{zz} =$ Moment of inertia about the z axis

As there is symmetry $I_{zz} = I_{yy}$

- **DIMPLES AND SPRING**

The dimples and the spring represent the connection between the fuel rod and the spacer grid. Due to the contact between the surfaces of the fuel rod with both the dimples and the spring, two different forces appear: the tangential force and the normal one. These forces are modeled by using two ANSYS elements that are used for the dimples, as well as for the spring. However, as the stiffness of the dimple is higher than the spring stiffness, the values of the parameters of the element are not the same.

- The normal contact depends on the value of the normal force applied on the contact element. While the normal force exists as it compresses the spring element, the contact will exist. The normal force causes two possible states: gap open or closed.

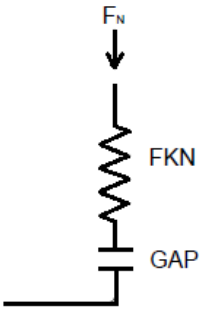

Figure 4. 3. *Representation of normal contact for contact elements in ANSYS.*

- The tangential sliding between the fuel rod and the dimples or spring is represented by a friction sliding element that depends on the status and has a hysteretic behavior, thus it is nonlinear and non-conservative. The tangential force causes two different possible states: sticking or sliding contact. With the presence of a positive normal force, the contact will be stick until the value of the tangential force exceeds the maximum friction force, which is μF_N.

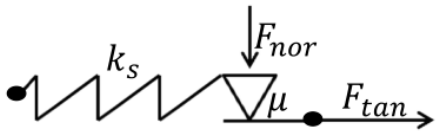

Figure 4. 4. *Representation of tangential contact for contact elements in ANSYS. [10]*

In order to define the elements used in the model, the stiffness of the dimples and the spring and also the initial normal force for the spring are needed. For each element, two stiffness are defined for both the tangential and the normal contact. These values are mainly based on the *(Lee, 1980)* paper [19].

F_N = Initial normal force for the spring

$K_{s,r}$ = Radial spring stiffness

$K_{s,t}$ = Tangential spring stiffness

$K_{d,r}$ = Radial dimple stiffness

$K_{d,t}$ = Tangential dimple stiffness

The definition of the different elements used in the model is completed by specifying the values of the KEYOPTIONS and the real constants according to the characteristics that each of them have.

COMBIN40 : Normal contact for the 2D model

The set-up of the COMBIN40 element is only relevant for the 2D model description, as all the contact elements in the three dimensional model are modeled with CONTA178. As it was explained in the element definition from *Chapter 3*, for this model COMBIN40 is only composed of a gap and a spring (see *Section 3.3.1.*).

- KEYOPTIONS

KEYOPT(3) selects the unique degree of freedom for the radial contact element. In this case, according to the nodes and the coordinate axes definition, the radial direction corresponds to the Y axis, so the value of the KEYOPT(3) is fixed to 2. Similarly, if the desired direction was the X axis or the Z one, the key option would take a value of 1 or 3 respectively.

- REAL CONSTANTS

Regarding the real constants definition, and taking into account that just the contact capability of the element is required, only the initial gap size and the spring constant are needed to be defined. Moreover, to create an initial interference, as explained in *Chapter 3*, the gap must have a negative value.

As the radial stiffness of the dimples and the spring are not the same and the normal forces are also different due to the equilibrium of forces, the values assigned to GAP and $K2$ are not the same for the dimples and for the spring.

Spring

The initial normal force applied on the spring has a value of F_N and the spring constant equals the radial spring stiffness. Thus, the initial gap size and the spring constant are defined as:

$$GAP = -\frac{F_N}{K_{s,r}} \qquad \textit{Equation 4.3}$$

$$K2 = K_{s,r} \qquad \textit{Equation 4.4}$$

Dimples

Furthermore, the normal force applied on each dimple will be half the force applied on the spring, that is $F_N/2$ so that the structure is meeting the static equilibrium and the

spring constant must be the radial dimple stiffness. Accordingly, the initial gap and the spring constant will be:

$$GAP = -\frac{F_N/_2}{K_{d,r}} \qquad \textit{Equation 4.5}$$

$$K2 = K_{d,r} \qquad \textit{Equation 4.6}$$

CONTA178: Tangential contact for 2D model and contact element for 3D model.

For the 2D model implementation, CONTA178 friction element is used to represent the grid-to-rod tangential contact. However, as it is a 3D contact element that represents the contact and sliding between two nodes of different elements, the 3D model will be implemented only with CONTA178 contact elements. Hence, instead of having two different elements for the normal and tangential contacts, the same element represents both. As well as for COMBIN40, the definition of the element is done by setting up the KEYOPTIONS and the real constants values. Since there are differences between the real constant values for dimples and springs and the set-up of the KEYOPTIONS for the perpendicular planes, the element has four different definitions.

- KEYOPTIONS:

The keyoption configuration is the same for the dimples and for the spring. Some of the keyoptions that are used in the model are explained below.

When defining the gap size, the locations of the nodes are ignored and the gap size is only defined with the real constant GAP, so KEYOPT(4)=1. (See the description of KEYOPTION(4) in *Section 3.3.2*.)

The basis for the normal contact deserves special attention. In the 2D configuration case, the 3D fuel rod support is being implemented in 2 dimensions, thus, one must be careful when defining the contact normal element directions. For example, CONTA178 represents the tangential contact, so the basis for the contact normal that must be selected is the Z component of the nodal coordinate system, which corresponds to a value of 3 for KEYOPT(5).

On the contrary, in the 3D case, the normal direction will correspond to the normal direction of the contact surface, which varies for the different perpendicular planes. Consequently, CONTA178 must be defined twice, one for the elements located in the XY plane and another one for the ones in the XZ plane. Therefore, KEYOPT(5) will take a

value of 2 (y-axis) for the dimples and spring placed in plane XY and a value of 3 (z-axis) for the elements contained in plane XZ.

- REAL CONSTANTS

The real constant definition will be the same for the two dimensional model and for the three dimensional one. CONTA178 is only effective for the sliding characteristic if the normal force is positive. The initial gap size is calculated on the same manner as for COMBIN40, but here it is also necessary to determine the initial contact condition of the first sub step, that is done by setting the value of the real constant START to a value of 3, which means that at the beginning the contact is closed without sliding ($\mu \neq 0$), as it was explained in the CONTA178 description of *Section 3.3.2*. Moreover, the values of FKN and FKS are defined as the radial and the tangential stiffness respectively, that are $K_{d,r}$ and $K_{d,t}$ for the dimples and $K_{s,r}$ and $K_{s,t}$ for the spring (see *Dimples and spring* of *Section 4.1.1.1*).

4.1.1.2. Model constraints

Once the elements are defined and the structure of the model has been drawn, the model must be constrained. This requires the nodes that connect the contact elements with the grid cell to be fixed (the nodes number that must be constrained change depending on whether it is the 2D or 3D model according to *Figures 4.1* and *4.2*) . Also, the displacement along the X direction of the fuel rod nodes to be restricted, so that the fuel rod does not fall down. Finally, for the 2D model, Z direction needs to be blocked. This z coordinate constraint will be removed for the 3D model case.

4.1.1.3. Implementation of the solution algorithm

After the definition of the model, the solution implementation of the model will be described. The final purpose of this section is to simulate the nonlinear and hysteretic behavior of the fuel-rod support. First of all the study of the different phases that are observed when the fuel rod is submitted to a rotation movement is done. With this purpose, for the 2D case, a moment on the Z coordinate will be applied to the central node of the fuel rod, which is node 3. The moment applied to the fuel rod will be increased from 0 Nm to 1 Nm for the loading and then decreased again until 0 Nm for the unloading. To have a complete view of the rotation behavior of the fuel rod support the loading and the unloading are also done in the opposite direction. For the 3D case, the same procedure is followed first for the two perpendicular planes separately, applying a moment around z and y axes respectively. After that, both moments will be applied at the

same time simulating then the vibration of the fuel rod within the spacer grid cell in three dimensions.

While implementing the model the ANSYS interface was used in order to check some variables and solutions. Specially, the *Miscellaneous* item of the $STAT$ was continuously consulted as it describes the contact status of an element at the end of every load step. This parameter shows if the gap is open, closed or if there is sliding contact.

4.1.2. Application of an axial preload.

In reality, during the reactor operation cycle there are some axial forces such as gravity or the hold down forces that are compressing the fuel assemblies. For that reason, it is interesting to see how these axial forces will affect the rotational mechanism of the fuel rod support. With this objective, the fuel rod was preloaded with different forces up to the maximum friction force, which is $4\mu F_N$ for the entire fuel rod support configuration. Then, the change on the nonlinear and hysteretic l behavior of the fuel rod rotation mechanism will be analyzed for the different preloads.

4.2. Second part: Evolution of the fuel rod support stiffness evolution under irradiation.

During the operation of the reactor, the springs and the dimples that make up the fuel rod support within the grid cell are being irradiated. Because of this irradiation the spring force decreases and it may lead to a spring separation from the fuel rod. The relaxation of the spring force is due to three main processes that are: the grid growth, the fuel-rod creep-down and the spring and dimple relaxation. Each of these phenomena is implemented in the ANSYS model on the following manner:

4.2.1. Implementation of the processes involved on the relaxation of the dimples and the springs.

Grid growth

Based on the *(Gunnar Wikmark, 2009)* document and using the grid growth curve for ZIRLO™ cladding material as a function of the burn-up in the reactor, the experimental data that is used in this model is obtained.

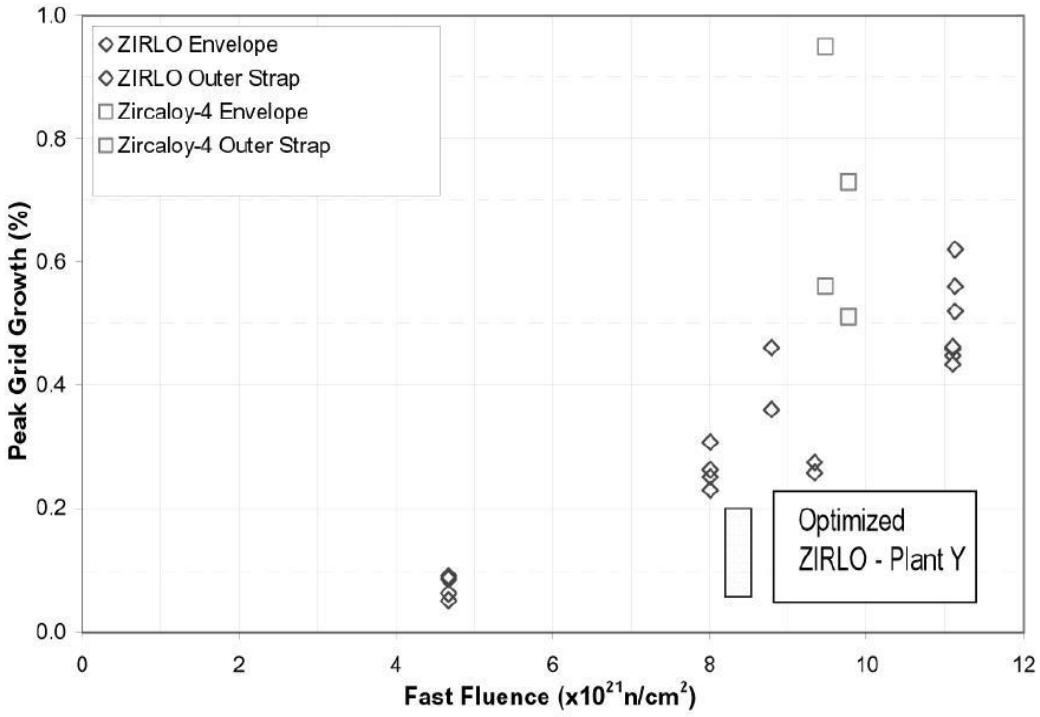

Figure 4. 5. *Grid growth as a function of fast neutron fluence for ZIRLO material of spacer grids.*

Using Matlab, the experimental data given in *(Gunnar Wikmark, 2009)* is fitted to a power series curve according to the grid growth law that is proposed in the *(Billerey, 2004)* paper.

$$\varepsilon = (aT + b){\Phi_t}^n \qquad \textit{Equation 4. 7}$$

With:

Φ_t : Fast fluence of the grid.

a, b, n : Constants

T : Temperature of the grid.

Neglecting the temperature, the grid growth law will be:

$$\varepsilon = b \cdot {\Phi_t}^n \qquad \textit{Equation 4. 8}$$

The resulting grid growth data dependent on the fluence is:

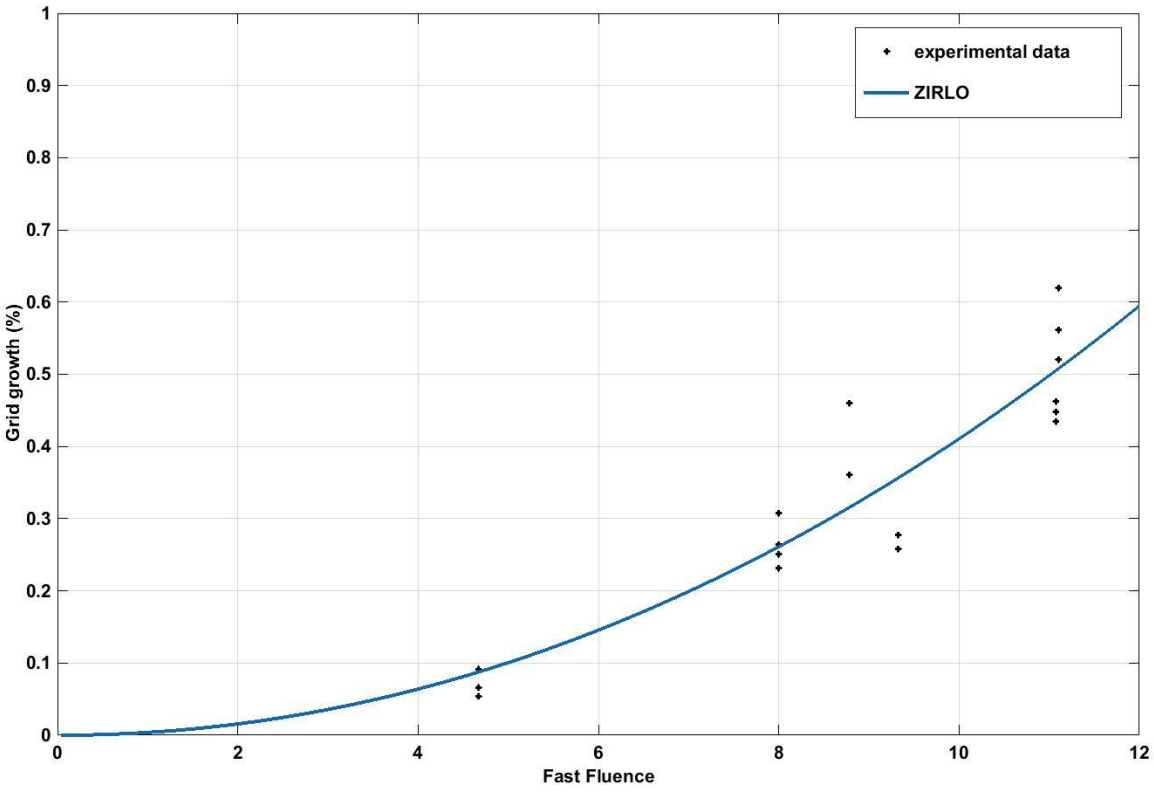

Figure 4. 6. *Grid growth curve obtained from the experimental data in Figure 4.5*

And the values of the constants, with a 95% confidence bounds, are:

$$b = 0.003835$$
$$n = 2.03$$

Finally, the axial plastic displacement due to the grid growth is calculated as follows:

$$Plastic\ displacement_{grid\_growth} = pitch \cdot a\ (\phi_t)^n \qquad \textit{Equation 4. 9}$$

Fuel-rod creep-down

The fuel rod creep down is calculated by a fuel performance code using a value of the flux of $\phi = 1.13 \cdot 10^{14}\ n/cm^2 \cdot s$. The data is obtained as a function of the operation time of the nuclear cycle, or in other words as a function of the burnup. Moreover, all the values are calculated for the mid grid position, specifically for the 5^{th} grid. Nevertheless, for the creep-down over the cell, the data must be multiplied by a factor of two, as the data that is provided refers to the radial creep-down.

The relaxation of the spring force is modelled for the mid grid position within the fuel assembly because there is where the highest flux is.

Creep law for spring and dimple relaxation

Due to the simplicity of the implementation, an explicit time integration approach has been used. Explicit methods make possible the calculation of variables for one time instant as a function of the previous values of the variables. These methods assume that the conditions at the beginning of a time step to be constant over the time step. The integration is carried out forward so that is why the used method is called forward Euler method. It allows calculating the approximate value of a parameter for $t + i$ by solving a linear approximation.

$$\dot{x_\iota} = \frac{x_{i+1} - x_i}{\Delta t} \quad \rightarrow \quad x_{i+1} = x_i + \dot{x_\iota} \cdot \Delta t \qquad \textit{Equation 4. 10}$$

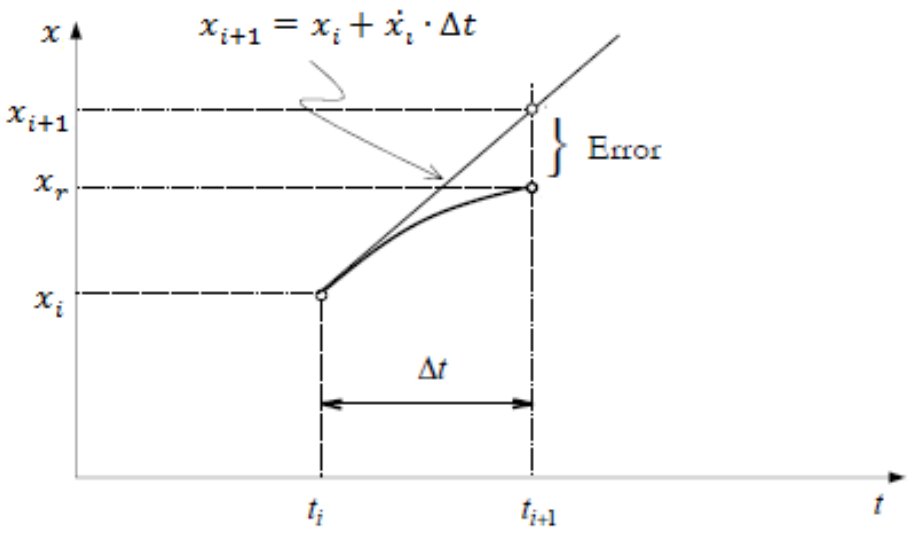

Figure 4. 7. *Explicit time integration. Forward Euler method.[21]*

From *Figure 4.7* it can be deduced that the bigger the time step, the bigger the error will be. Therefore, the limitation for the time step choice will be the desired accuracy of the solution. Specifically, the algorithm implemented here for calculating the plastic creep was based on *(Rust, 2011)*.

For the creep of the dimples and the spring under irradiation, the creep law from *(P.Yvon, 1998)* is used.

$$\varepsilon_{cr} = A\, e^{\frac{-Q}{RT}}\, \sigma_{el}\ \phi_t{}^{n} = C\, \sigma_{el}\, t^{n} \qquad \textit{Equation 4. 11}$$

With:

A, n: Constants

Q: Activation energy

R: Gas constant

T: Temperature

ϕ_t: Fast neutron fluence

σ_{el} : Elastic stress

In this case, the irradiation creep strain increment for a time step is calculated as:

$$\Delta\varepsilon_{cr} = \dot{\varepsilon}_{cr}(t) \cdot \Delta t \qquad \textit{Equation 4. 12}$$

As the aim of this study is to obtain the evolution curve of the spring preload force with the operation time, and the only quantities that are known before irradiation are the initial spring normal force F_N, the spring stiffness k and the elastic displacement Δu_{el}, some transformations are made in order to calculate the plastic displacement depending on the known quantities [24].

First of all, a linear spring can be considered to be equivalent to a linear bar element with the same modulus of elasticity E_{el}, cross-sectional area of $Area$ and an initial length of u_{ini}.

$$k = \frac{Area\ E_{el}}{u_{ini}} \qquad \textit{Equation 4. 13}$$

Expressing the stress and strain in terms of absolute quantities and inserting them into the creep law equation, the formula will be:

$$\Delta u_{cr} = A\ e^{\frac{-Q}{RT}} {\phi_t}^n\ F_{el} \frac{u_{ini}}{Area} \qquad \textit{Equation 4. 14}$$

Finally, expanding the formula with the elasticity modulus E_{el} , the creep law has the following expression:

$$\Delta u_{cr} = A\ e^{\frac{-Q}{RT}} {\phi_t}^n\ F_{el} \frac{E_{el}}{k} \qquad \textit{Equation 4. 15}$$

For the creep of the dimples and the spring, the stiffness k will be the radial one, $K_{d,r}$ and $K_{s,r}$ respectively. The temperature T is assumed to be the average temperature in the reactor core, which is 315℃ and the flux $1.13 \cdot 10^{14}\, n/cm^2 \cdot s$ that is based on the flux value used for the fuel rod creep down calculations. The values of A, Q/R and n are taken from the *Yvon (1998)* document:

$$A = 1.5 \cdot 10^{-18}\, cm^{1.6}/MPa$$
$$Q/R = 4700\ K$$
$$n = 0.8$$

The modulus of elasticity is interpolated with Matlab from the Modulus of Elasticity Zircaloy-4 dependent on the temperature graph presented by *(Whitmarsh)*.

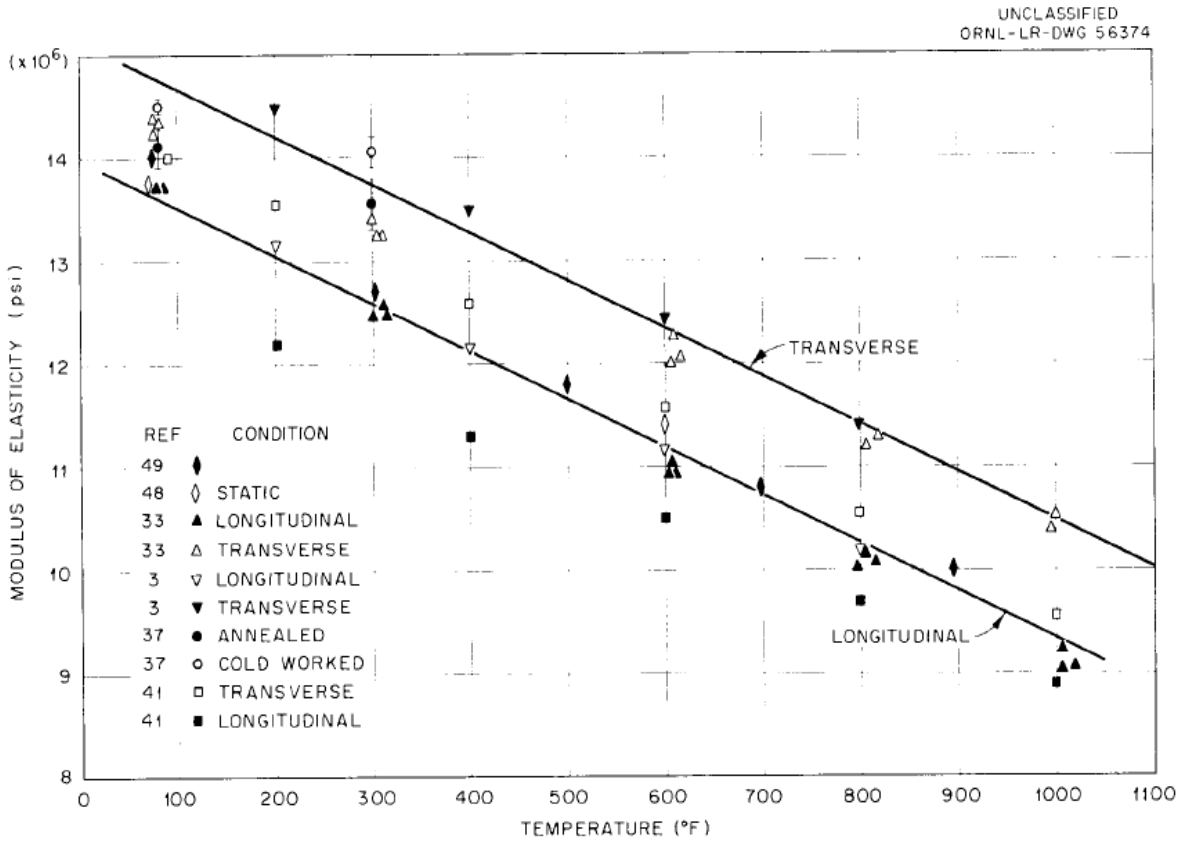

Figure 4. 8. *Modulus of elasticity of Zircaloy-2 as a function of temperature*.

For the operation temperature ($T = 315℃ \approx 600°F$) and according to *Figure 4.8*, the Modulus of Elasticity has a value of $11.1772 \cdot 10^6\ psi$ which results in:

$$E_{el} = 77.0641\ Gpa$$

With all these values, the creep law as a function of the normal force and applying the forward Euler method, the plastic displacement due to the irradiation creep effect for a time step will be:

$$u_{cr}(t + \Delta t) = u_{cr}(t) + \Delta u_{cr} \qquad \textit{Equation 4. 16}$$

Where $u_{cr}(t)$ corresponds to the irradiation creep for the previous time step and Δu_{cr} the increment of the creep effect for the present time step.

Taking the derivative of the creep law, the creep rate is:

$$\Delta \dot{u}_{cr} = A\ e^{\frac{-Q}{RT}} F_{el} \frac{E_{el}}{k}\ \phi^n\ n\ t^{n-1} \qquad \textit{Equation 4. 17}$$

And then:

$$\Delta u_{cr} = A\ e^{\frac{-Q}{RT}} F_{el} \frac{E_{el}}{k}\ \phi^n\ n\ t^{n-1} \cdot \Delta t \qquad \textit{Equation 4. 18}$$

The solution will be obtained with an iterative process where Δt will correspond with the time increment applied on each load step, t will be the current time and the value of the remaining normal force in the spring F_{el} will be obtained at the end of every load step and will be introduced into the next time step calculation. Thus, at the beginning the normal force there will be the preload force of the dimples or the spring and from that moment, the value of the force will be provided by the ANSYS calculation.

To obtain a realistic solution, both the relaxation of the dimples and the spring are taken into account in both planes XY and XZ, so the study is done with the 3D model.

Since the algorithm has been thought following the explicit forward Euler method, the total irradiation creep for a specific time step has to be saved in a variable ($u_{cr}(t)$) , so that it can be used for the following time step calculation.

Furthermore, one must be consistent with the variable parameters used for the calculation of the displacements along the Y and Z directions. The normal force that is provided by the program has to correspond with the displacement calculation, for example, for the plastic displacement of the spring on the plane XZ, the stiffness will be $K_{s,r}$ and the normal force will be the force on the spring element placed between nodes 5 and 8.

Accordingly, all the irradiation creep calculations that are solved for every load step and taking a constant C_{abs}, which evolves all the constants present on the equation are:

With:

$$C_{abs} = A\ e^{\frac{-Q}{RT}}\ \phi^n\ n\ E_{el} \qquad \textit{Equation 4. 19}$$

Plastic displacements due to irradiation creep for the springs and dimples:

$$Plastic\_displ_{i,j} = C_{abs} \cdot \frac{F_{j,k,v}}{k_{i,r}} \cdot t^{n-1} \cdot \Delta t \qquad \textit{Equation 4. 20}$$

With:

$i = s, d$ Referring to spring or dimple
$j = y, z$ Normal direction of the element
$k = 21, 25, 42, 43, 44, 46$ Element number
$v = 1, 2, 3, 7, 8, 9$ External node number (spacer grid nodes)

4.2.2. Implementation of the solution

The remaining normal force of the spring as the spring relaxes at the end of a load step can be expressed as a function of the total plastic displacements mainly caused by the three processes explained before, the initial displacement and the spring stiffness

$$F_N = \left(u_{ini} - \sum u_{plastic}\right) \cdot k_s \qquad \textit{Equation 4.21}$$

Usually the relaxation of the normal force in a spring is modeled as a decrease of the elastic stiffness. Nevertheless, for the ANSYS elements that are used in this model, the real constants cannot be changed during the simulation. Hence, the stiffness parameters are bound to be constant. As an alternative method, the relaxation of the normal force is modeled by moving the different nodes a certain distance, which will be the total plastic displacement. This displacement is the sum of the plastic deformations due to the growth of the grid cell, the creep-down of the fuel rod diameter and the irradiation creep of the dimples and the springs that are summed up for every load step . The sum of these three displacements will be applied towards such a direction that the contact elements will decompress, so that the dimples and the springs, which are initially preloaded with a normal force will relax as the distance between the elements extremes increases (see *Figure 4.9*).

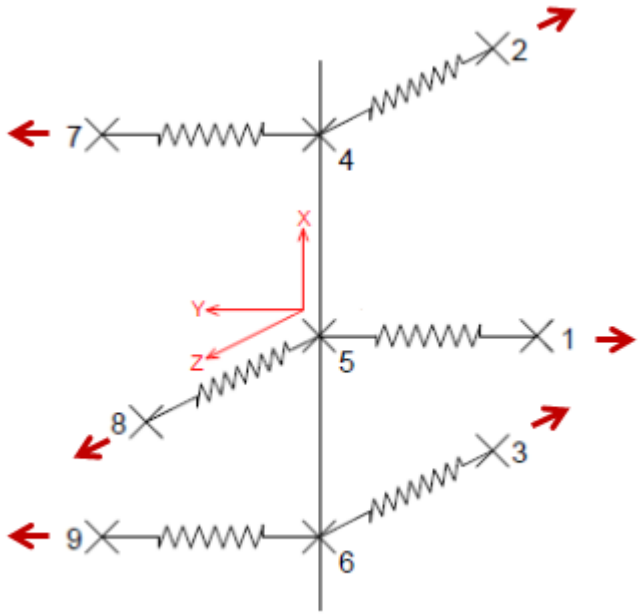

Figure 4.9. *Schematic application of plastic displacements to the nodes connecting with the spacer grid.*

As both the plastic displacements due to the grid growth and the creep-down are calculated for the total diameter, the displacement applied to one of the nodes will be half the total one of each of these quantities.

$$u_{growth} = \frac{Plastic\ displacement_{grid\_growth}}{2} \qquad \textit{Equation 4. 22}$$

$$u_{creep-down} = \frac{Plastic\ displacement_{creep\_down}}{2} \qquad \textit{Equation 4. 23}$$

However, pure irradiation creep relaxation does not induce any movement, but it relaxes the spring force. Thus, as the stiffness of the dimples is higher than the one of the spring and the fuel rod must stay motionless at the same central position, the following correction must be done:

$$u_{creep,s} = u_{creep}\frac{2k_{d,r}}{(2k_{d,r} + k_{s,r})} \qquad \textit{Equation 4. 24}$$

$$u_{creep,d} = u_{creep}\frac{k_{s,r}}{(2k_{d,r} + k_{s,r})} \qquad \textit{Equation 4. 25}$$

This compensation must be done according to the plane of the displacement and the contact element. So finally the displacements will be:

$$Plastic\ displacement_{i,j} = u_{growth,i,j} + u_{creep-down,i,j} + u_{creep,i,j} \qquad \textit{Equation 4. 26}$$

With:

$i = s, d$	Element type (spring or dimple)
$j = y, z$	Direction of the displacement

Once the total displacements for both springs and the four dimples have been calculated, they are applied to the respective nodes, which are the connecting points between the contact elements and the grid (nodes 1,2,3,7,8 and 9). By applying a displacement to a node, its location changes on the quantity of the total displacement applied and towards the direction that is specified with the displacement command.

4.2.3. Time step selection

With the objective of proving that the time hardening algorithm implemented in the model reproduces the analytical solution, a comparison between the model and the analytical solution is carried out. Moreover, comparing the analytical solution with the relaxation curve for different choices of the time step allows the user to select an appropriate time step that provides an accurate solution. This task was done for a simple configuration consisting of one single spring connecting two fixed nodes. As the algorithm corresponds only to the irradiation creep effect, this is the only process that is taken into account for the spring force relaxation here.

The elastic force of the spring can be analytically expressed as:

$$F_{el} = F_N - \Delta u_{creep} \cdot k \qquad \textit{Equation 4.27}$$

Taking the derivative:

$$\frac{dF_{el}}{dt} = -\Delta \dot{u}_{creep} \cdot k \qquad \textit{Equation 4.28}$$

And knowing that the displacement due to the irradiation creep is:

$$\Delta \dot{u}_{creep} = A \; e^{\frac{-Q}{RT}} F_{el} \frac{E_{el}}{k} \; \phi^n \, n \, t^{n-1} \qquad \textit{Equation 4.29}$$

Collecting all the constant parameters with:

$$B = A \; e^{\frac{-Q}{RT}} E_{el} \, \phi^n \, n \qquad \textit{Equation 4.30}$$

The differential equation is then:

$$\frac{dF_{el}}{dt} = -B \cdot F_{el} \cdot t^{-0.2} \qquad \textit{Equation 4.31}$$

Finally, solving the differential equation:

$$F_{el} = C \cdot e^{-B \cdot \frac{t^{0.8}}{0.8}} \qquad \textit{Equation 4.32}$$

Substituting the initial condition, the final expression results in:

$$F_{el} = F_N \cdot e^{-B \cdot \frac{t^{0.8}}{0.8}} \qquad \textit{Equation 4.33}$$

With this formula, it is possible to implement the evolution of the normal force of the spring caused by the creep due to irradiation and then, compare the result with the simple model ones for different choices of the time step.

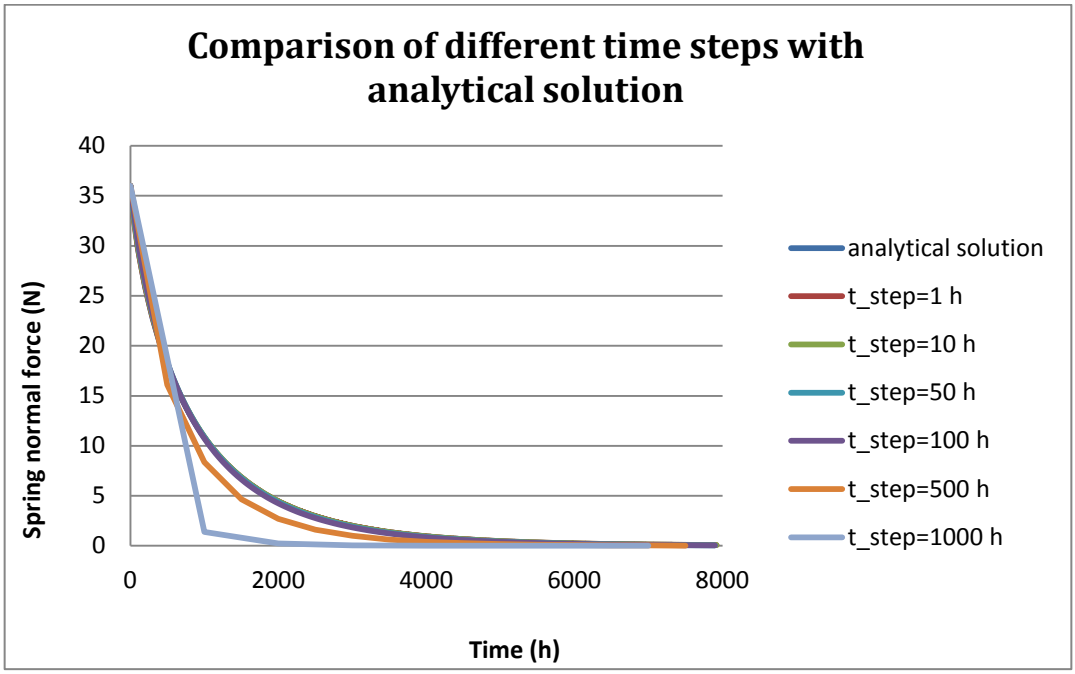

Figure 4. 10. *Spring relaxation due to irradiation creep. Comparison of different time steps with analytical solution for a simple configuration.*

As it can be seen in the plot above, with a time step around 500 h or more the solution will not be reliable. Nevertheless, time steps up to 100 h provide a solution that seems to be close to the analytical one. For estimating the accuracy of the solution for time steps up to 100 h, another plot is attached below where the differences between the curves can be seen.

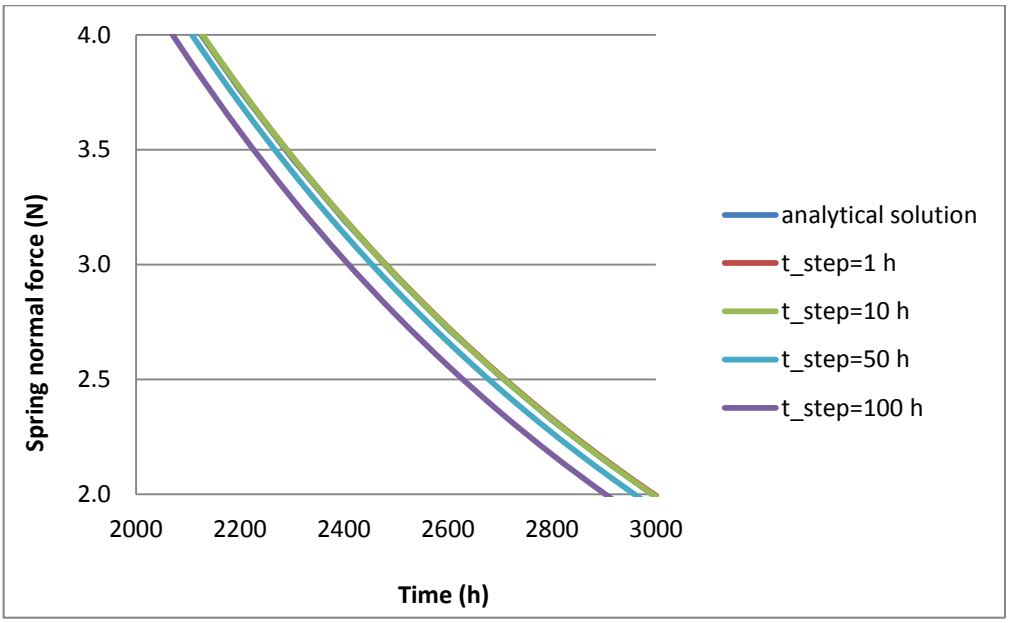

Figure 4. 11. *Zoom of Figure 4.10.*

Time step	Simulation time		
	2000 h	5000 h	7900 h
1 h	0.209 %	0.222 %	0.239 %
10 h	0.294 %	0.403 %	0.932 %
50 h	1.23 %	5.05 %	7.88 %
100 h	4.18 %	11.17 %	17.1 %

Table 4. 1. *Deviations of the results for different simulation times and different time steps*

Although the most accurate solution would be that obtained with the lower time step (1 h in this case), the simulation would be slower. Hence, relying on the deviation values of *Table 4.1*., it was considered that using a time step of for example 10h would provide a reliable solution while the running would not be that slow.

Moreover, the figure below shows a comparison between the characteristics of the deviations from the analytical solution different time steps for the relaxation of a single spring connected between two nodes. *Figure 4.12* shows the characteristic curves of the solution deviations from the analytical solution for different time steps which could not be differentiated in *Figure 4.10*.

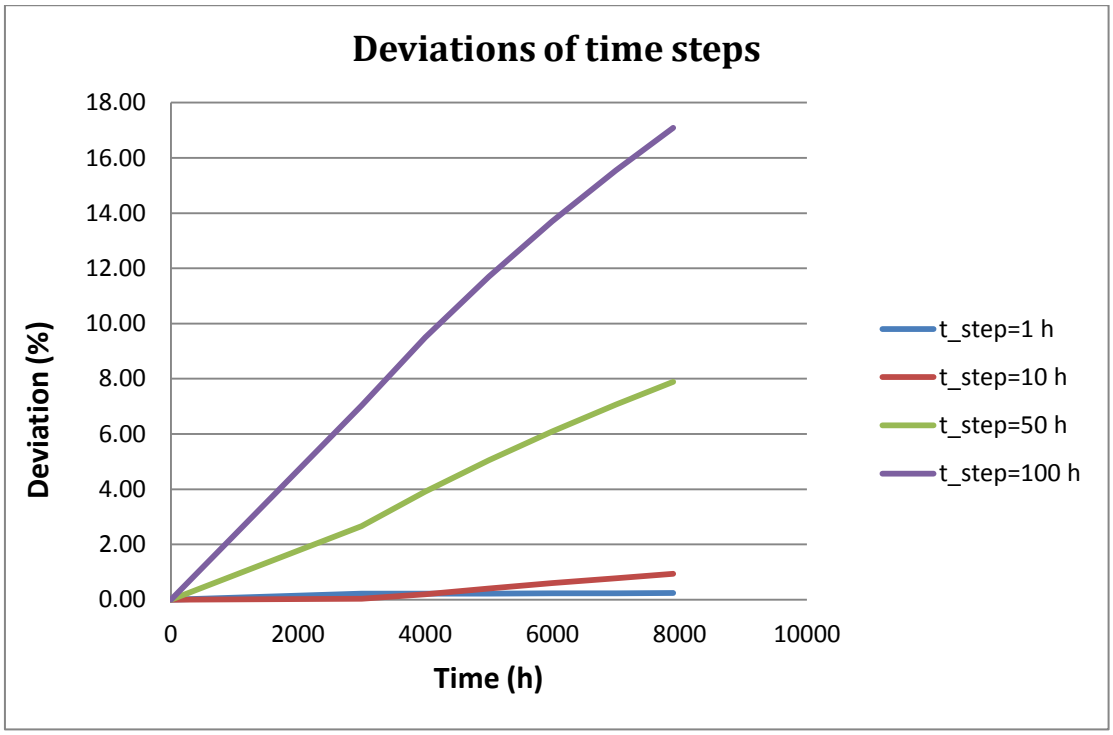

Fugure 4. 12. *Characteristic of time steps deviations.*

5. Results

5.1. Part 1: Nonlinear and hysteretic behavior of fuel rod support.

5.1.1. Fuel-rod support model in 2D

As it was explained in *Section 4.1.1.3*, for the loading of the fuel rod support rotation, a moment about z-axis from 0 Nm up to 1 Nm was applied. With rotation about that axis the rotation plane is the one defined by axes x-y. The figure below shows the rotational characteristic obtained with the 2D model that is presented in this work.

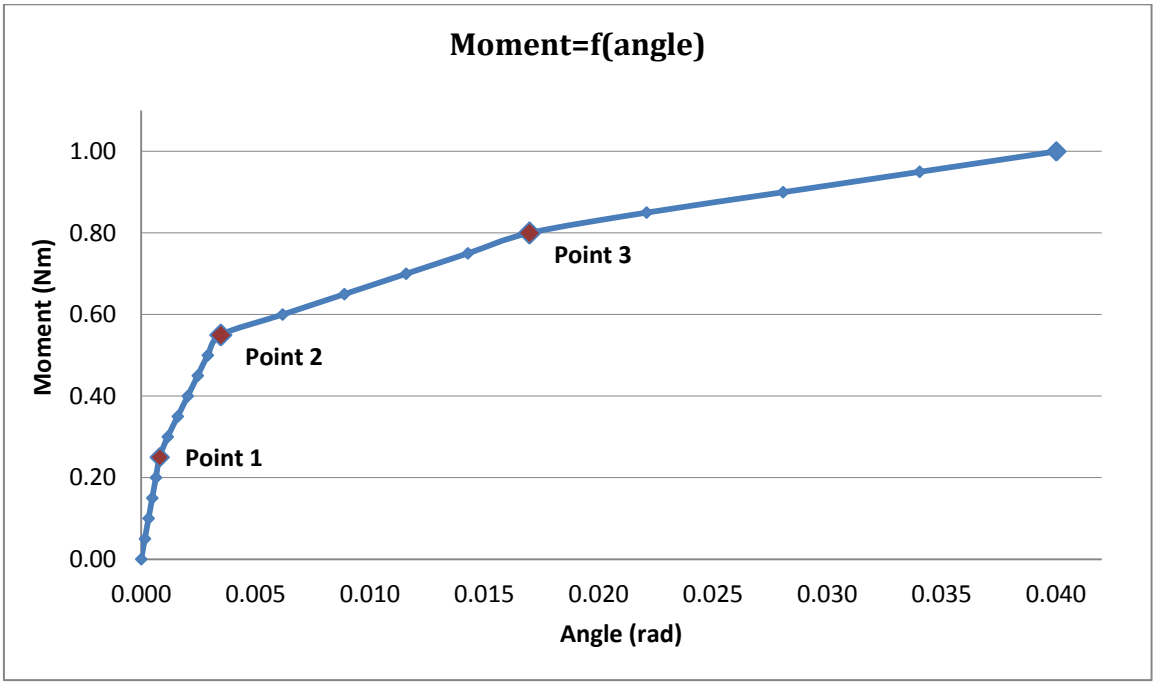

Figure 5. 1. *Rotation characteristic for rotation mechanism loading in 2D model*

In *Figure 5.1*, one can identify four different slopes that correspond to the four phases explained in *Chapter 2* for the rotation loading of the fuel rod support within the spacer grid. The limiting points between phases are included in the plot. According to the physical explanation of the curve, at first both the dimples and the spring would be loading, the spring at rest, the rotation point central and the contact between elements on the perpendicular plane and the fuel rod would be sticking. As the moment increases, from ***Point 1***, the fuel rod would slide over the perpendicular dimples while the both dimples belonging to the rotation plane would continue to load. This is because of the normal movement of the dimples placed in the rotational plane. Furthermore, the spring will stay at rest and the rotation point central. This situation would continue until the dimple that is being unloaded will be completely decompressed (***Point* 2**). Then, a gap would open between that dimple and the fuel rod and due to that, the rotation point would

not be central any more. Consequently, the spring will be loading. Finally, as the rotation continues, the spring keeps loading and at one point (***Point 3***), the normal tangential force of the perpendicular spring would reach the maximum force for sliding and the fuel rod would slide over the spring too. The rest of the elements would be the same as for the previous phase: a gap between one of the dimples and the fuel rod would exist, the other dimple would be loading, the contact with perpendicular dimples would be sliding and the rotation point would not be in the center. Thus, the symmetry would still be broken.

The table down below compares the values obtained with the ANSYS model and the analytical values resulting from the equilibrium equations of the different phases explained above. While analytical values are obtained by solving the equations presented in the *Rotation of the fuel rod section* of *Chapter 2*, model points that define the successive thresholds between phases have been remarked in *Figure 5.1*.

Phase		Analytical values	Model results	Deviation (%)
1a-1b	θ_1(rad)	0.00082	0.00080	2.44
	M_1(Nm)	0.265	0.250	5.66
1b-2a	θ_2(rad)	0.00327	0.00348	6.42
	M_2(Nm)	0.5486	0.5500	0.25
2a-2b	θ_3(rad)	0.0173	0.0170	1.73
	M_3(Nm)	0.870	0.800	8

Table 5.1. *Comparison between model results and analytical ones and the correspondent deviations for the loading curve of the 2D rotation model.*

From *Table 5.1*, it can be said that, since the deviation between model and analytical results is no larger than 8%, the model reproduces quite well the analytical behavior of the rotation characteristic for the fuel rod.

The complete loading and unloading curve in one direction and in the opposite one looks like this:

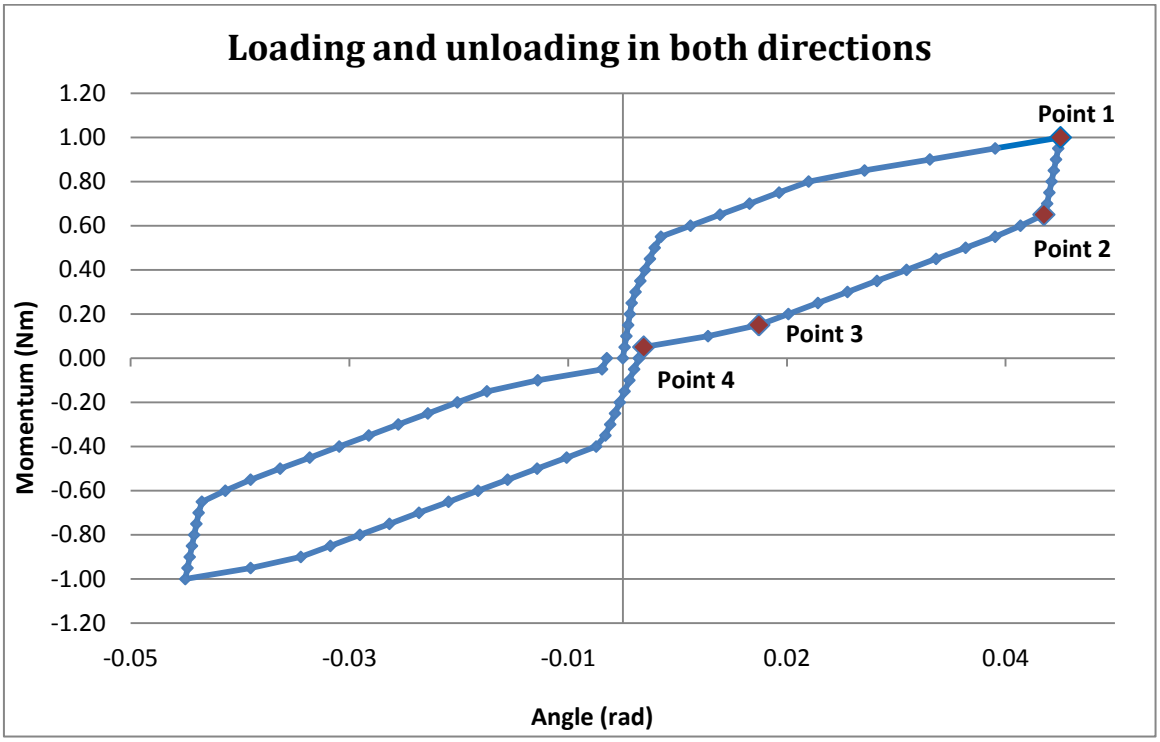

Figure 5. 2. *Complete loading and unloading of fuel rod rotation for 2D model in both directions about z-axis.*

Figure 5.2 shows the nonlinear hysteretic characteristic of the fuel rod interacting with the spring and the two arches holding it in place within the spacer grid cell. The loading steps are the ones that have been already explained. Nevertheless, since at the end of the loading the fuel rod has shifted over the dimples and the spring and had also lost contact with one of the dimples, the rotation center has changed and thus, the unloading process does not follow the same path as the loading. Although the unloading curve of the fuel rod support seems to follow the same phases as it did for the loading, the actual state of the contact elements during these phases is not the same.

In order to understand the phases happening during the unloading of the rotation, it is useful to have in mind the four phases of the loading that were explained in *Section 2.1*. Especially, the reader should remember the state of the contact elements at the end of the loading (*Phase 2a* in the description of the rotation of the fuel rod in *Section 2.1.1*).

The first steep slope of the unloading is due to the reduction of the moment (from ***Point 1*** to ***Point 2*** in *Figure 5.2*). At the end of the loading, the rod was sliding over both dimples and spring in a plane perpendicular to the rotational plane. Hence, tangential forces of these elements had their maximum values. When the moment decreases, normal force of the dimple which is still in contact and the normal force of the spring decrease too, as they are being decompressed. Consequently, tangential forces in the perpendicular plane decrease below the maximum force until sliding. Therefore, tangential stiffness of both spring and dimples are again active, so the fuel rod is again in sticking contact with all the elements. On the other hand, the gap between one of the dimples and the fuel rod remains open while the other dimple and the spring maintain the contact with the rod.

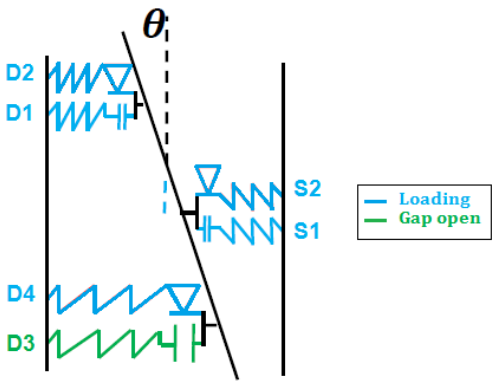

Figure 5. 3. *Representation of ANSYS elements states for the 2D model during rotation of the fuel rod. First phase of the unloading process.*

At one point, as the moment continues decreasing, the fuel rod slides over the lower dimple which is placed on the perpendicular plane to the rotational one (***Point 2*** of *Figure 5.2*). During loading the tangential behavior of both dimples was the same but now, since the center of rotation has changed, there is no symmetry any more. For that reason, the tangential force of the perpendicular dimple which is located in the lower part of the fuel rod increases faster than the one of the upper dimple. As a consequence the fuel rod slides only over the lower perpendicular dimple. Furthermore, in this phase (second slope of the unloading curve) the rest of the tangential contacts remain sticking, the gap opens and the spring and dimple in contact with the fuel rod.

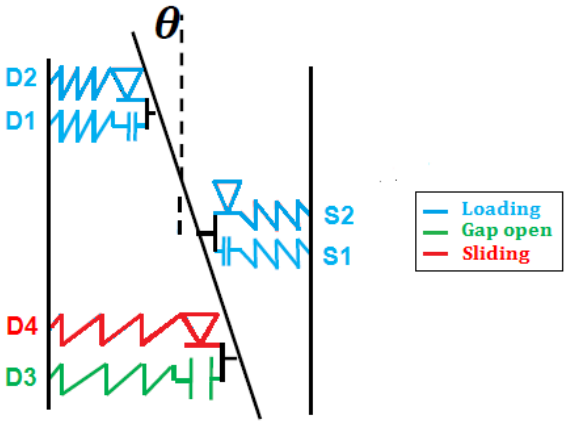

Figure 5. 4. *Representation of ANSYS elements states for the 2D model during rotation of the fuel rod. Second phase of the unloading process.*

The second phase lasts until the tangential force exceeds the maximum one of the upper dimple and then, the fuel rod slides over both dimples in a plane perpendicular to the rotation one (from ***Point 3*** to ***Point 4*** in *Figure 5.2*). During this third phase, the gap remains open and the rest of the normal contacts closed.

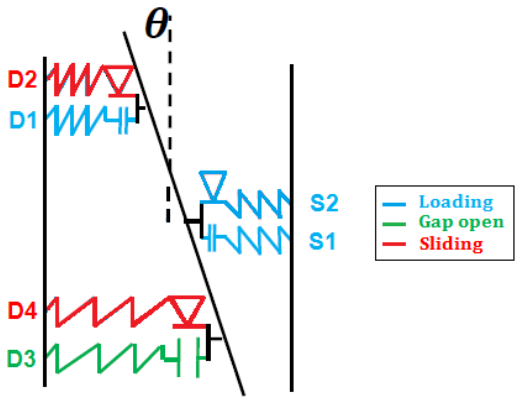

Figure 5. 5. *Representation of ANSYS elements states for the 2D model during rotation of the fuel rod. Third phase of the unloading process.*

Finally, as the moment applied is close to zero, the rotational angle is close to zero so the gap closes (***Point 4*** in *Figure 5.2*). The tangential force of the perpendicular spring continues increasing until it reaches the maximum force and then the fuel rod also slides over the spring. In this moment, the fuel rod is in contact with all the contact elements and slides over both perpendicular dimples and spring.

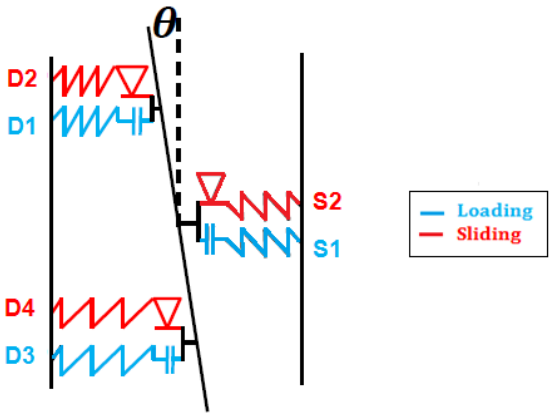

Figure 5. 6. *Representation of ANSYS elements states for the 2D model during rotation of the fuel rod. First phase of the unloading process.*

5.1.2. Fuel rod support rotation characteristic with 3D model.

First of all only one moment is applied to one of the perpendicular axis (z-axis) and the evolution of the curve is then compared to that of the 2D model.

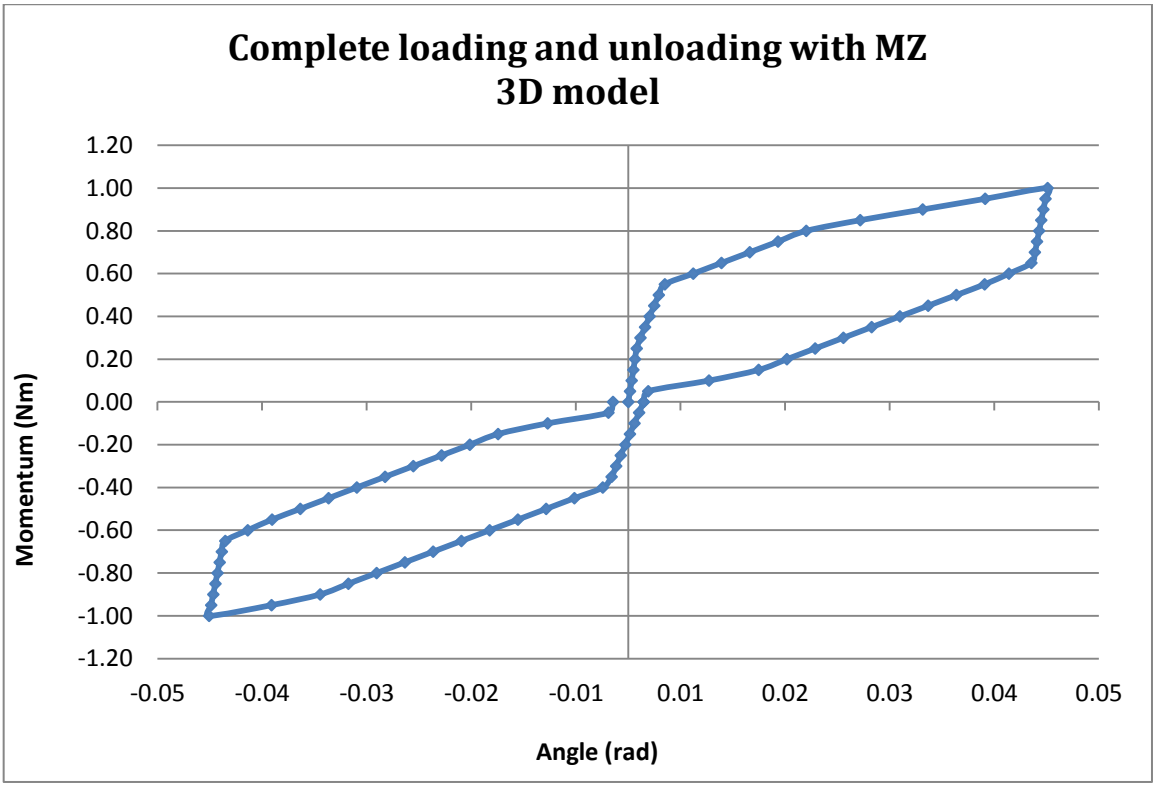

Figure 5. 7. *Complete loading and unloading of fuel rod rotation for 3D model in both directions about z-axis.*

Even though there is only one graph included, the 3D test for the rotation of the rod in one plane was carried out in the two perpendicular planes, applying the moment about z or y axes respectively. Both graphs showed the same hysteretic shape, which is none other than the result of the two dimensional model.

After the two dimensional test, the complete loading-unloading process was implemented for the three dimensional model in both perpendicular planes simultaneously.

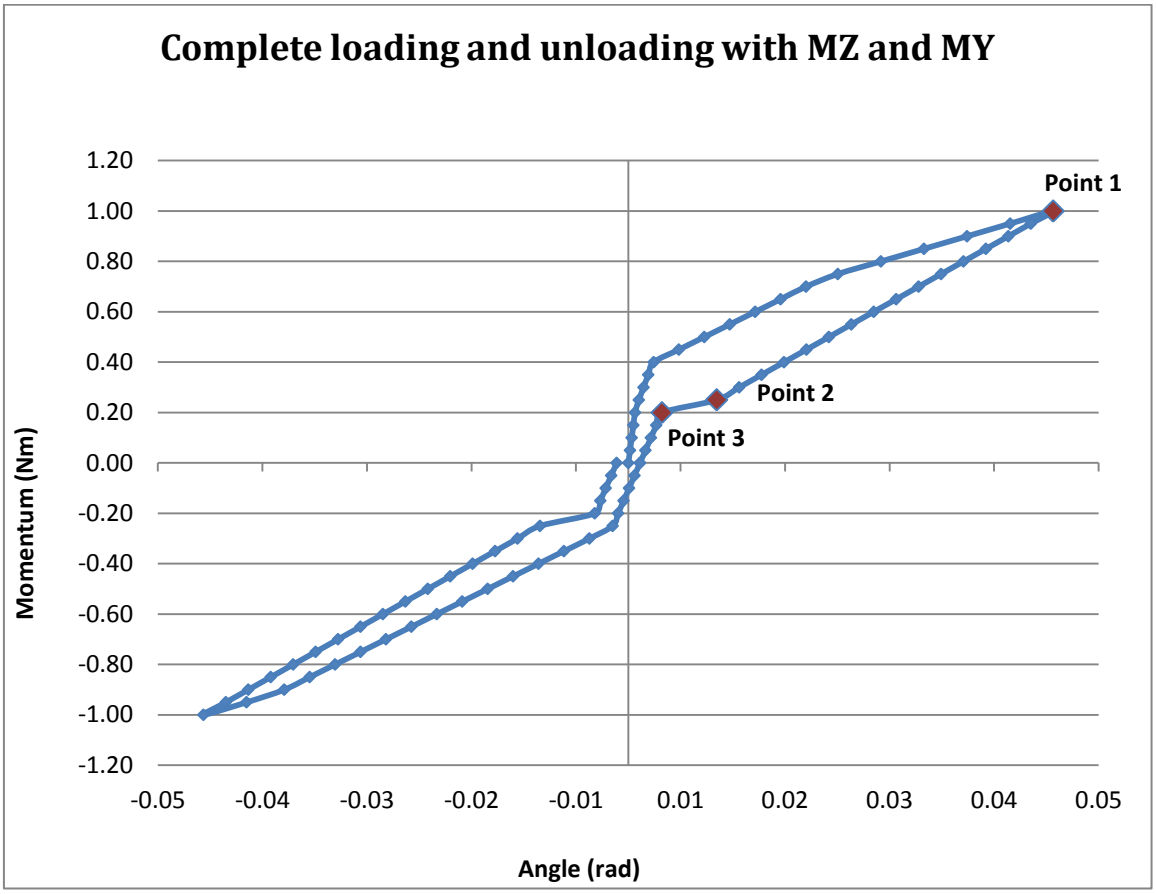

Figure 5. 8. *Complete loading and unloading of fuel rod rotation for 3D model in both directions about z and y axes.*

For the loading part of the fuel rod support, the results plotted in *Figure 5.8* are similar to the loading curve of a single plane. However, the unloading curve looks different. The most remarkable difference is observed at the beginning of the unloading part. Before reading the description of the unloading phases it is recommended to review the four loading phases that were explained in *Section 2.1.1*. Then, the reader can better understand what is really happening as the moments applied to the fuel rod are being decreased. Furthermore, in order to simplify the explanation the state of the contact elements will be described for each phase referring to those dimples and spring that are located in one of the perpendicular planes. Nevertheless, the behavior of the elements contained on the other plane is exactly the same.

As it happened with the unloading in 2D, once the applied moment starts to decrease, the tangential stiffness become active again and all fuel rod contacts are sticking (see the description of the unloading process in *Section 5.1.1*). The slope of the first unloading phase of the 3D model (from ***Point 1*** to ***Point 2*** in *Figure 5.8*) is less steep as the one of the 2D model (from ***Point 1*** to ***Point 2*** in *Figure 5.2*). The reason of this divergence is that now, there is no contact between the fuel rod and the lower dimples (in any of the perpendicular planes). Therefore, since the first unloading slope is strongly influenced by

the lower dimple tangential contact, for the 3D model case the first slope resembles more the second slope of the 2D model unloading curve, where the fuel rod was sliding over the perpendicular dimple. As both moments continue to decrease, the gap closes and the fuel rod slides over all contact elements (from ***Point 2*** to ***Point 3*** in *Figure 5.8*). However, this phase is short when compared with the previous one. During the last phase (from ***Point 3*** in *Figure 5.8*) of the unloading the contact with the dimples is sliding while the one with the spring becomes sticking.

5.1.3. Rotation characteristic of the fuel rod support with an axial preload.

The aim in this section is to investigate and explain how the presence of an axial force affects the rotation characteristic of the fuel rod support. With this aim, an axial preload was applied on top of the fuel rod. This force was incremented from $0N$ to $F_{fr,max}$, which is the maximum friction force for the total fuel rod support within the grid cell. Hence, the 3D model was used.

$$F_{fr,max} = 4\mu F_N$$

The presence of the axial preload is expected so that the phases where the fuel rod is not sliding over the dimples and the spring will be shorter. As this force becomes larger, the margin for the sliding becomes shorter too because the tangential force increases. Then, the margin that the tangential force has for sliding is smaller.

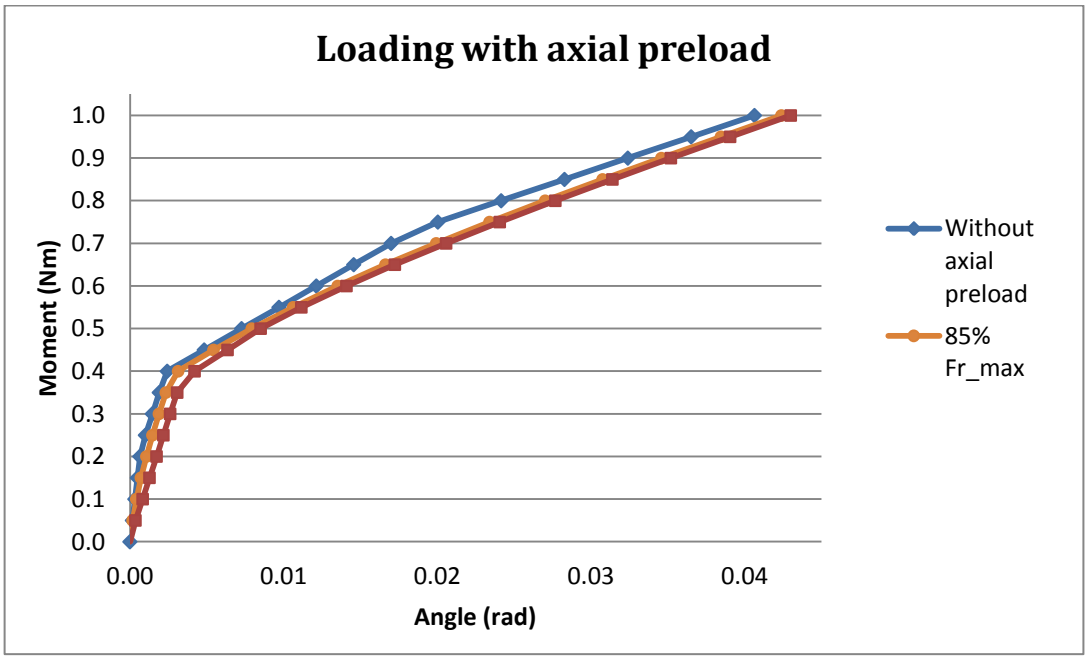

Figure 5. 9. *Loading curve of 3D model with the presence of different axial preloads.*

This graph shows the loading part for the rotation evolution of the support mechanism of the fuel rod for several values of the preload. As the differences between the curves is not so clear, attached is another graph that shows a zoom of this figure for the first changes of slopes.

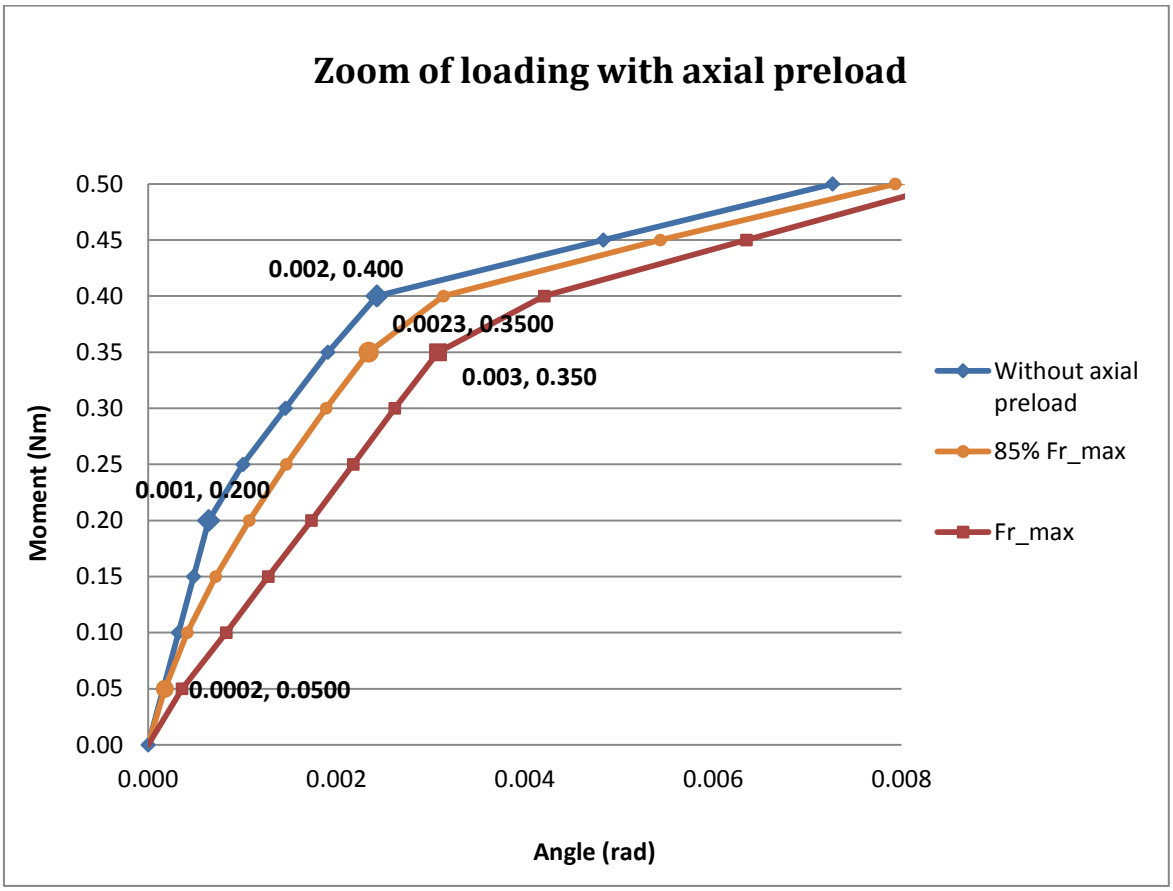

Figure 5.10. *Zoom of Figure 5.5.*

As it was expected, as the axial preload increases, the threshold force until sliding is lower and thus, the first phase becomes shorter until it completely disappears. Relying on the equations included in the Pure Penalty method explanation of *Chapter 3*, the evolution shown in *Figure 5.10* can be explained.

For each of the perpendicular planes, the tangential force can be expressed as:

$$F_s = \sqrt{F_x^2 + F_a^2} \qquad with\ \ a = y, z \qquad \textit{Equation 5.1}$$

Taking into account the complete support mechanism with the two springs and four dimples sliding will occur for:

$$\sqrt{F_x^2 + F_a^2} = 4\mu F_N \qquad \textit{Equation 5.2}$$

Hence, in the absence of axial preload, the force on y or z direction has a wider margin until sliding. As the axial force increases, the margin for the F_a term becomes lower. Consequently, as the normal forces on the springs and the dimples are related to the applied moment, the fuel rod slides over the dimples and the spring for a lower moment.

Regarding the curves on the previous figure, the first phase of the rotation for the orange curve is around 75% shorter than it is for the blue one. The second phase, which corresponds to the dimples sliding, is then larger for the presence of an axial force. In the figure it can be seen that in the curve without axial preload, the fuel rod slides for a moment of 0.2 Nm and with 85 % of the maximum sliding force it slides with 0.05 Nm. One can identify parallel slopes with the same physical facts occurring during rotation. In the case of the maximum friction force applied, the first phase does not exist. Looking at *Equation 5.2* , if the axial force equals the maximum friction force for sliding, there is no margin left for either the force in z or y directions. In *Figure 5.10* this translates in the absence of phase one, so from the beginning of the rotation, the fuel rod is sliding over the dimples. One can see that the slope of the red curve from the origin until 0.35 Nm is parallel to the slopes of the second phase of the other two curves (from 0.2 Nm to 0.4 Nm for the blue one and from 0.05 Nm to 0.35 Nm the orange one).

This explanation for the sliding threshold of the dimples can be extended to the one of the spring that corresponds with the point between the slopes of phases 2a and 2b. According to this, when the axial preload equals the maximum friction force, only two slopes seem to be clearly differentiated in the rotation characteristic of the fuel rod support, what means that only two different phases will occur and they will correspond with the sliding phases.

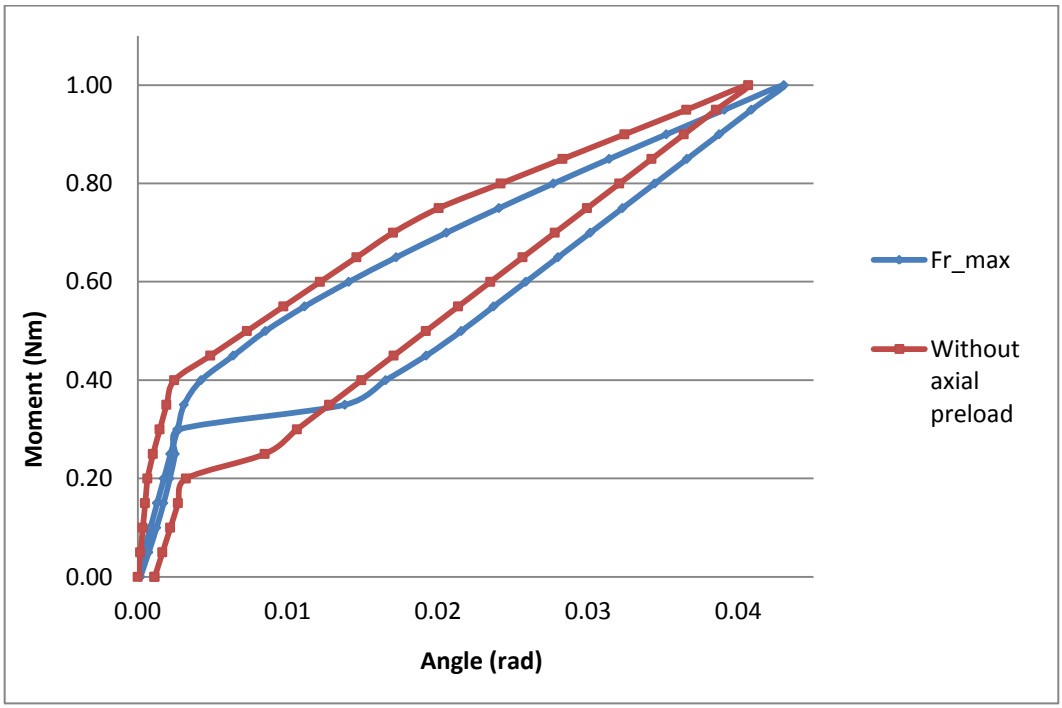

Figure 5. 11. *Complete loading and unloading for maximum friction force and without axial force.*

In the plot above it is easier to distinct the change in the evolution of the fuel rod support with and without an axial preload. The figure shows loading and unloading for the 3D case without axial preload and with the maximum one and applying both moments to axes Y and Z.

In reality, fuel rods are submitted to axial forces, as they are compressed by the hold-down force that is applied before starting the reactor to prevent FA from elevating during operation. Hence, if this axial preload surpasses the sliding limiting force, only two phases will be present while loading and the fuel rod will be sliding always over the dimples or both the dimples and the springs.

5.2. Part 2: Relaxation of the spring force under irradiation.

5.2.1. Model solution

In order to compare these model results with the reference curves from previous studies regarding the spring force relaxation under irradiation, all the results are presented as a function of the burn-up rate of the reactor.

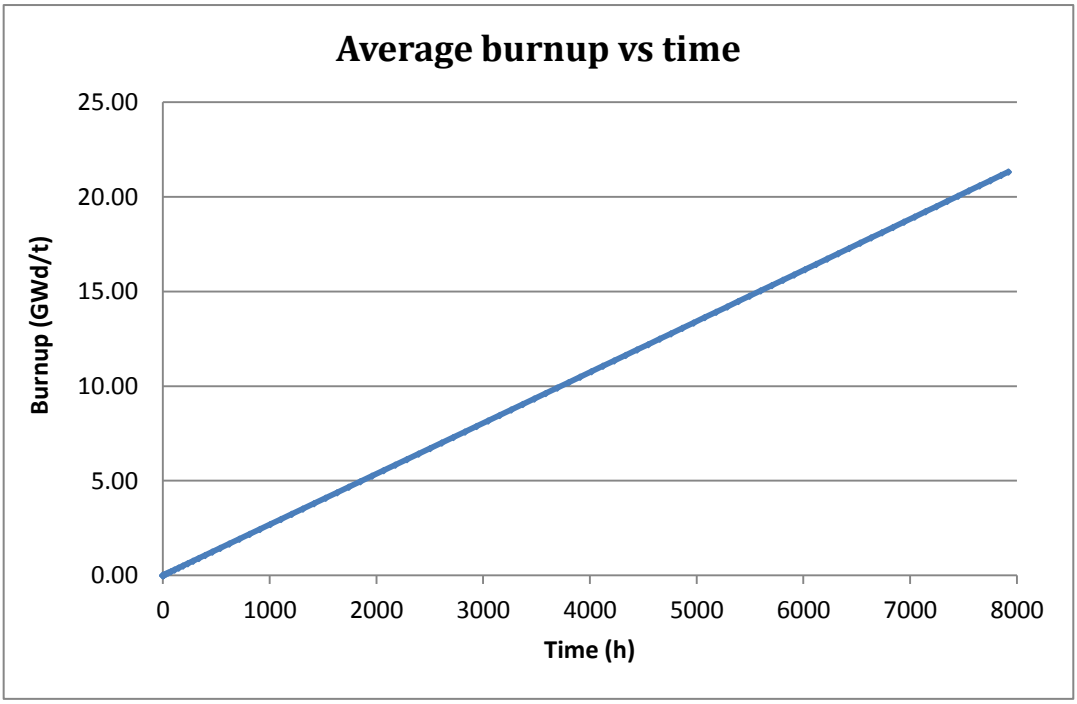

Figure 5. 12. *Plot of burn-up vs time*.

As for our reference case there is nearly a linear relation between the reactor operation time and the burn-up, the results can be plotted as a function of either the time or the burn-up.

Regarding the implementation of the three main processes that affect the degradation of the spring force during the reactor operation, each of these processes was considered separately before considering the total effect on the normal force. The intention was to see the three additive terms on its own to have an idea of the effect that it will have in the total degradation of the spring force.

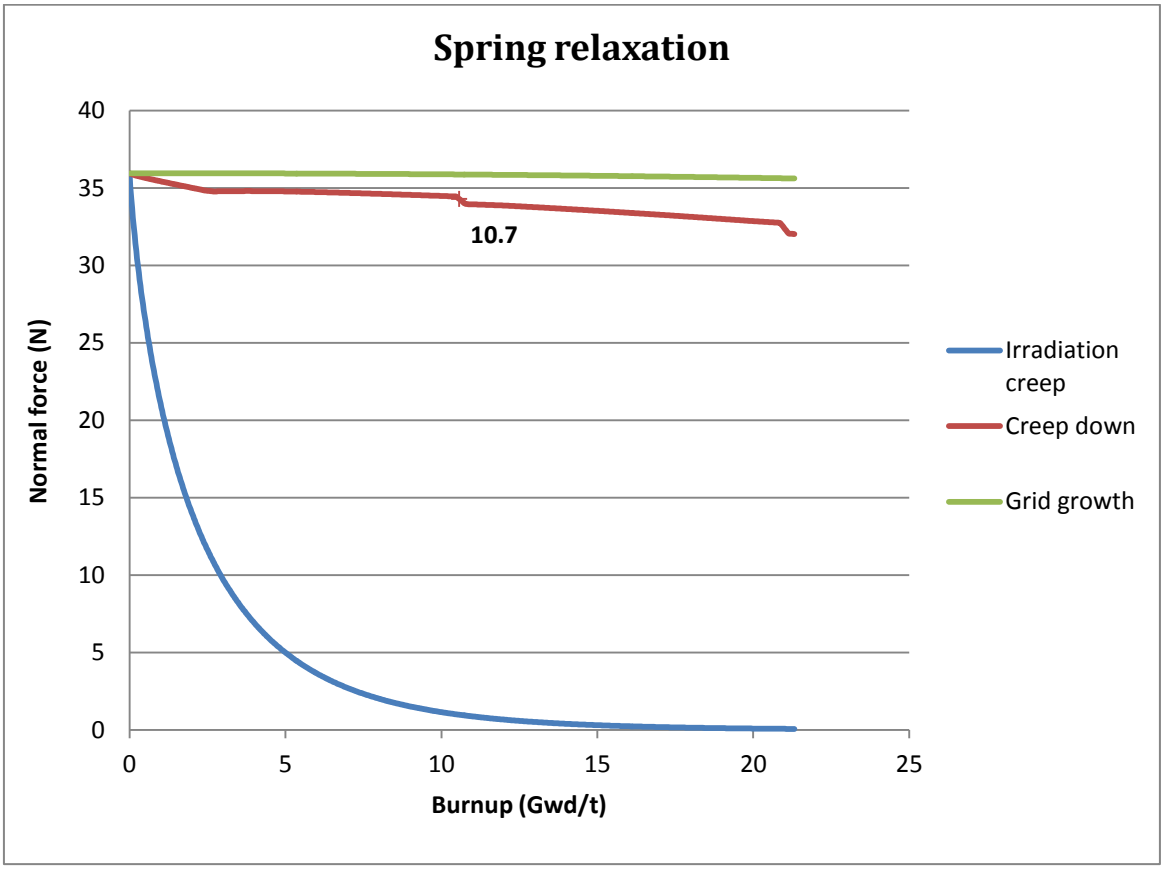

Figure 5. 13. *Relaxation of the spring force due to irradiation creep, spacer grid growth and clad diameter creep down. Three processes separately.*

The figure above shows the effects of the three processes involved in the spring relaxation separately. The normal force in *Figure 5.13* is the remaining normal force of the spring as it is being relaxed. The most influent one is the effect of the irradiation creep law. This curve has an exponential evolution according to the formula of the irradiation creep law (*Equation 4.33*) with an exponential factor depending on the time. On the other hand, considering that the simulation was run for one year of the reactor operation, the relaxation caused by the grid growth is not so significant when compared with the relaxation caused by irradiation creep. On the diametric creep down evolution there are two relatively abrupt drops, one at the end of the reactor operation and another one around half of the total burn up. These drops are due to the specific power history used in the fuel performance code from which the creep down data was obtained.

The total spring normal force degradation including the effects of the grid growth, the irradiation creep law and the reduction of the fuel rod diameter is featured.

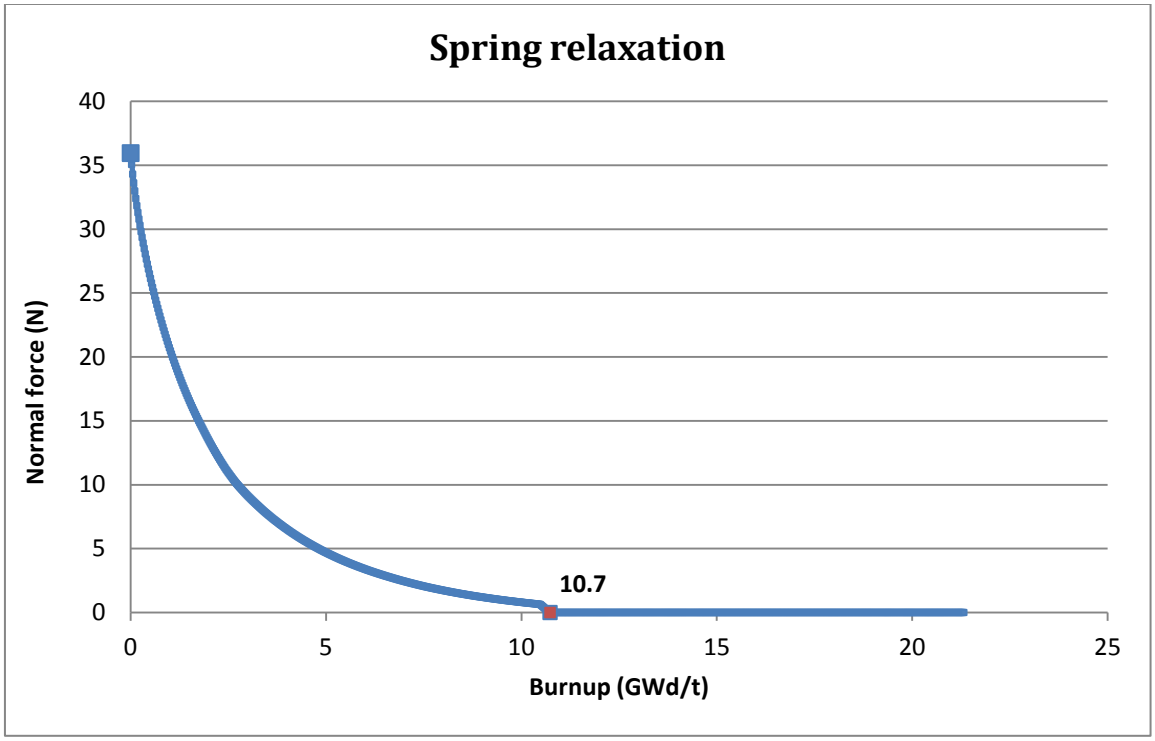

Figure 5. 14. *Relaxation of the spring force due to irradiation creep, spacer grid growth and clad diameter creep down. All processes acting.*

After analyzing the effects of the different processes, it was expected that the evolution of the spring force taking into account all of them together would be strongly influenced by the irradiation creep law. And that is exactly what is shown in the figure above. Besides that, the spring gets totally relaxed before it did only with the irradiation creep effect, because of the effects of both the grid growth and the development of the clad diameter under irradiation. Moreover, the same drop that was observed on the creep down evolution (see *Figure 5.13*) appears here, where the normal force drops to zero. The burn-up value is around 10.7 GWd/t twhich corresponds to 4000 h of operation. When the normal force becomes zero, the spring is completely decompressed and consequently, a gap between the fuel rod and the spacer grid opens. Furthermore, as the irradiation creep effect is related to the spring force and the actual term that is counted for the relaxation due to it depends on the normal force of the spring. Then once the force disappears the spring is completely relaxed. However, the other two processes continue active governing the gap size.

As a complement, the evolution of the gap opening was plotted, as shown in *Figure 5.15*.

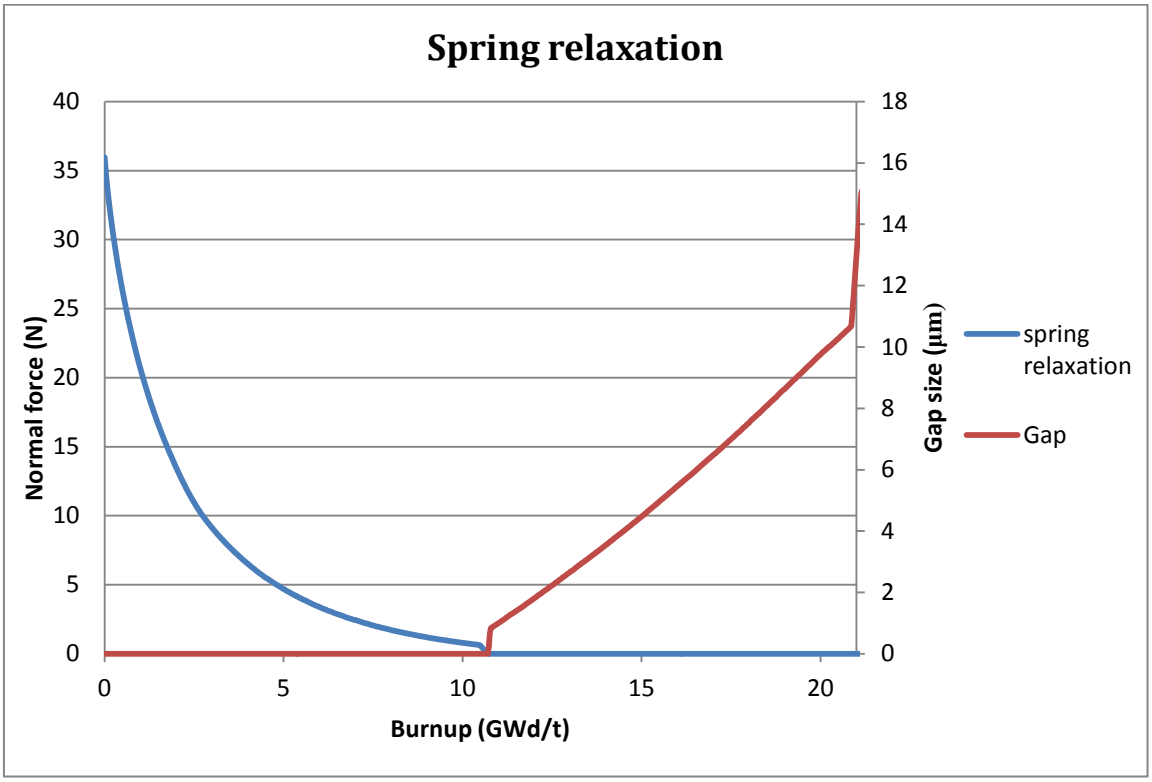

Figure 5. 15. *Relaxation of the spring force and evolution of the gap size.*

The gap remains closed as long as the spring is compressed and opens when it becomes zero. At that time it is observed an abrupt step which is also observed at the end of the simulation and is due to the evolution of the clad diameter decrease.

5.2.2. Parametrical analysis

As an additional study, a parametrical analysis is included. The aim of this apart is to see how the variation of some parameters involved in the process may affect the evolution of the spring normal force during the operation of the reactor. Concretely, the effect of a change of the irradiation creep process and the spring stiffness are studied.

Variation of the creep law effect

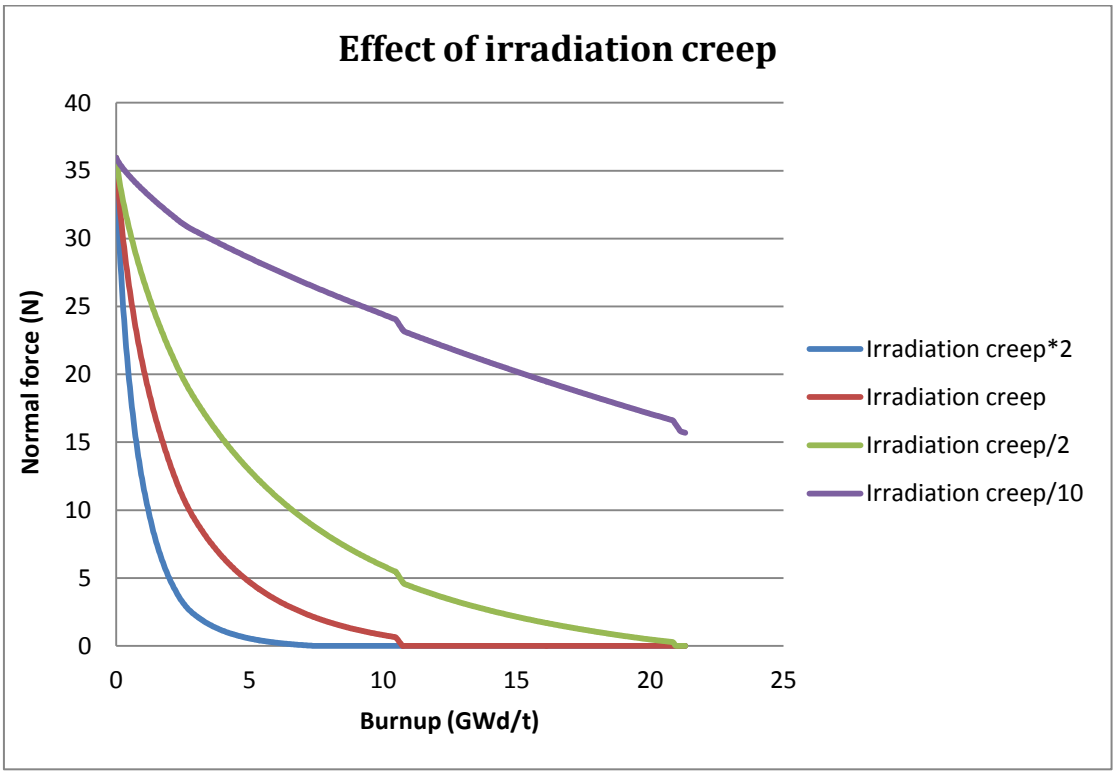

Figure 5. 16. *Effect of irradiation creep law effect variation on spring relaxation.*

Regarding the previous results, it is known that the irradiation creep law has a strong effect on the degradation of the spring force. Hence, when this process becomes less important, the relaxation of the spring is slower. On the contrary, as this term increases its value, the decrease of the spring force is faster. This study directly manipulates the time constant of the exponential decrease of the spring force. So increasing the creep, the exponential decrease becomes faster and accordingly, decreasing it, the time constant is increased and the exponential is slower.

Variation of the spring stiffness

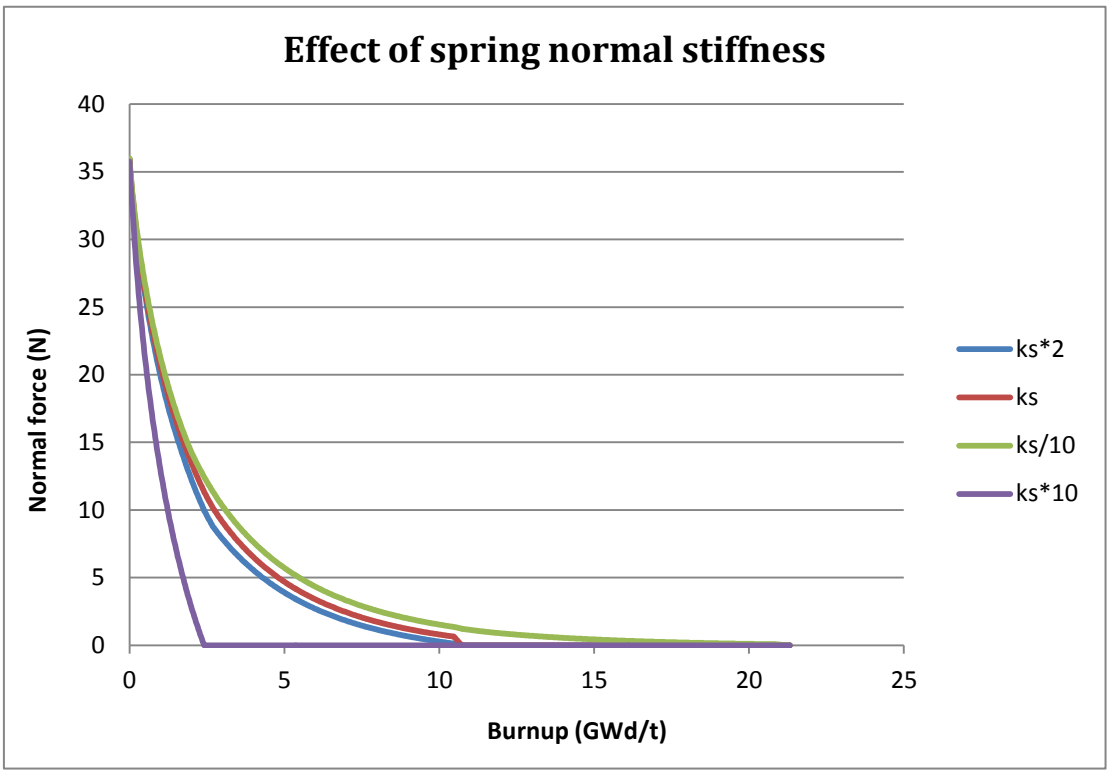

Figure 5. 17. *Variation of the spring relaxation with several values of the spring normal stiffness.*

In *Section 4.2.3* the exponential equation that governs the exponential expression for the irradiation creep law was developed. There, the reader can see that the exponential curve does not depend on the spring stiffness, since it was cancelled out. Therefore, a change of the spring stiffness does not affect the evolution of the exponential. However, both the presence of the spacer grid growth and the diameter creep down of the clad have an effect on the relaxation of the spring.

While applying a compressing force over a spring, the total length of the spring decreases from its initial value. Moreover, the variation of the spring length is proportionally related to the applied force by the spring stiffness. The effect of both growth of the spacer grid and reduction of the clad diameter is translated into an elongation of the spring. Thus, the force related to these processes, which is actually decompressing the spring, can be also expressed as a function of the spring stiffness and the induced elongation. Besides that, the correspondent displacements to each of these two processes are independent of the spring stiffness. For that reason, since the value of these displacements remain unchanged for a certain time step, if the spring stiffness has a higher value, the value of the force will also increase. Consequently, the spring will relax faster. Similarly, the force will decrease for a lower value of the

spring stiffness and therefore the relaxation will be slower. This is the reason for which in *Figure 5.17* variations on the relaxation curve of the spring are observed.

6. Conclusions

The objective of this work was to implement a reliable tool that could predict FA bow on a small scale (rod to spacer grid connection). The reason is that an accurate knowledge of the mechanical behavior of the fuel rod support can help to predict and prevent possible operation and safety problems of nuclear power plants. This thesis focuses on the static mechanical aspects of the fuel rod support. The study has been carried out in two different parts: the study of the rotational behavior of the fuel rod within the spacer grid cell and the evolution of the support springs force under irradiation.

The first step was the implementation of a two dimensional model of the fuel rod support, which consists of a combination of springs and dimples placed in two perpendicular planes. This model was based on the one dimensional FEM model implemented with ANSYS APDL simulation software that is presented in [10]. The evolution of the fuel rod support rotation has been simulated with both2D and 3D models. However, the bulk of the complete analysis has been done only using the 3D model.

In the 2D study, four different phases during the fuel rod rotation have been observed, which correspond with the phases that had already been described by previous studies. For each phase, the state of the contact between the spring and the dimples that support the fuel rod coincides with the rotation phases that have already been experimentally observed. In addition to the rotation loading, the complete hysteretic behavior has been plotted and both the loading and unloading phases of the rotation have been described. The model results show good agreement with the physical events that happen during the fuel rod rotation. Thus, the validity of the 2D model is demonstrated.

After the 2D analysis, the same test was carried out for the 3D model, obtaining similar results. Furthermore, the 3D configuration was also submitted to the rotation of the fuel rod about two perpendicular axes simultaneously and the rotation evolution was described. In this case, the loading curve resembled to the one of the 2D model while the unloading curve was considerably different. This difference of the unloading behavior was due to the gap opening at the end of the loading in both perpendicular planes. When the gap exists in both planes, there is neither sticking nor sliding contact between the fuel rod and the perpendicular dimple which mainly governs the hysteretic behavior.

As a compliment to the fuel rod rotation study, a last test was done. This test consisted of the same previous test (evolution of the fuel rod rotation) but with the addition of an axial preload. The reason is that in reality, fuel assemblies are submitted to axial forces so the results of this test provided a more realistic simulation of the fuel rod rotation. It was observed that, as the axial preload was closer to the maximum frictional force for the whole configuration, the slopes of the curve that correspond to the sliding of the rod over

the dimples or the spring became calmer and shorter. The reason is that, the increase of the axial force reduces the margin for the tangential sliding either in z or y directions.

The second part of the work was designed for the study of the spring force evolution under irradiation for the 3D model. It was assumed that the three most influent processes in the relaxation of the spring force are: the growth of the spacer grid, the reduction of the clad diameter due to creep (diameter creep-down) and the creep of the springs and dimples under irradiation. Initially, the relaxation of the spring force was simulated taking into account each of the three processes separately. The results showed that the most influent process for the degradation of the normal force was the irradiation creep. However, when considering all the processes involved in relaxation, results show that the effect of both creep down and grid growth accelerated the relaxation process. According to the results, the spring would be completely relaxed by 4000 h of the operation cycle, as was expected. In that moment, a gap would open between the fuel rod and the spring. The evolution of this gap is also included.

Finally, a parametrical analysis for the spring force relaxation was carried out. The results showed that an increase of the irradiation creep effect is translated into an acceleration of the normal force degradation. Similarly, a decrease of the irradiation creep will slow the relaxation of the force. The reason is that when the irradiation term carries more weight, the time constant of the exponential decreases and the exponential is faster. On the contrary, by reducing the irradiation creep weight, the time constant decreases and the exponential becomes slower. Besides that, a variation of the spring stiffness implied a slight change of the force relaxation curve, since it only impacts the relaxation caused by grid growth and creep down, which are actually less significant than the irradiation creep effect.

All the results that have been presented and discussed in this work show that the 2D and 3D model of the fuel rod support implemented in ANSYS predict with a good confidence, the rotational behavior of the fuel rod and the relaxation of the spring force under irradiation. Thus, since the rotational characteristic of the fuel rod within the spacer grid cell determines the mechanical response of the FA to lateral forces and the relaxation of the normal force in the springs implies a decrease of the FA stiffness, this model should be implemented into the complete FA model presented in [10]. This should allow the user to reach more accurate solutions for the bow analysis of the FA.

Acknowledgements

Above all I would like to thank Prof. Dr. Macián-Juan for giving me the opportunity to carry out this project in the Department of Nuclear Engineering. I have learnt a lot from his knowledge, expertise and extensive experience in the field of nuclear engineering.

I would like to express my deepest gratitude to Dipl. Ing. Andreas Wanninger for his guidance and disposition towards this work. I am thankful for his patience and for his generosity especially in assisting me with the project while always maintaining a positive attitude. I wish him all the best for his future. I also want to thank all the members of the department, for making my time here very pleasant, with a special mention to Dipl. Ing. Jamel Rhouma who has always showed his care for my work and personal motivation.

Furthermore, I would like to express my heartfelt love and thanks to my family, for always supporting me. Especially to my parents for providing me with numerous opportunities, not only educational but also personal ones. I also want to thank my sister María, for her priceless unconditional encouragement and positivity.

In addition, I want to thank all my friends in Munich, who have been a part of this wonderful experience, especially the four girls with whom I have been working with daily in the "PC-Raum" over the last six months. Their support and genuine friendship have made the last half year unforgettable.

Finally, I want to thank Greg O'Donnell for his continuous support, his useful advice, and above all for making my tough days during this time much better.

Bibliography

[1] *www.nucleartourist.com*. (n.d.). Retrieved Abril 2015, from http://www.nucleartourist.com/images/pwr-cycle.gif

[2] *www.photobucket.com*. (n.d.). Retrieved Abril 2015, from http://s244.photobucket.com/user/jpc24/media/PWR.jpg.html

[3] Pramuditya, S. (2014, April 14). Retrieved April 2015, from https://syeilendrapramuditya.wordpress.com/2009/04/14/standard-pwr-nuclear-fuel-assembly-17x17-technical-specification/

[4] Buongiorno, J. (2010). *CANES, Center for Advanced Nuclear Energy Systems*. Retrieved April 2015, from http://ocw.mit.edu/courses/nuclear-engineering/22-06-engineering-of-nuclear-systems-fall-2010/lectures-and-readings/MIT22_06F10_lec06a.pdf

[5] Grayson, J. (2011). *Control rods in nuclear reactors*. Retrieved from Stanford University: http://large.stanford.edu/courses/2011/ph241/grayson1/

[6] Andreas Wanninger, M. S.-J. (n.d.). Understanding Future Research Needs to Better Describe Fuel Assembly Bow in PWRs. Garching, Bayern, Germany.

[7] Stabel, J. H.-P. (1995, August). Fuel Assembly Bow: Analytical Modeling and Resulting Design Improvements. *Transactions of the 13th International Conference on Structural Mechanics in reactor Technology*. Erlangen, Germany.

[8] B. Levasseur, G. C. (2009, September). 3-D Modelling of Fuel Assembly bow for EDF PWRs. *Proceedings of Top Fuel*. Paris, France.

[9] Billerey, A. (2004). *Evolution of fuel rod support under irradiation - Impact on the mechanical behaviour of fuel assemblies*. Villeurbanne, France.

[10] Wanninger, A. (2015, January 16). Development of Computational Methods to Describe the In-Reactor Mechanical Behavior of PWR Fuel Assemblies. Garching, Bayern, Germany.

[11] S.Was, G. (2007). *Fundamentals of Radiation Material Science - Metals and alloys*. Springer.

[12] Murty, K. L. (2013). *Materials Ageing and Degradation in Light Water Reactors*. Cambridge, UK: Woodhead Publishing Limited.

[13] ANSYS, Inc. (2009). *ANSYS Parametric Design Language Guide*. Canonsburg, PA .

[14] Campinas State University, Brasil. (n.d.). *www.fem.unicamp.br*. Retrieved from http://www.fem.unicamp.br/~lafer/im437/Cap11.pdf

[15] ANSYS, Inc. (2012). *ANSYS Mechanical APDL Command Reference*. U.S.

[16] ANSYS, Inc. (2012). *ANSYS Mechanical APDL Element Reference*. U.S.

[17] *Pennsylvania State University, School of Engineering*. (n.d.). Retrieved Abril 2015, from http://engr.bd.psu.edu/davej/icons/beam-orient.PNG

[18] Günter Kessler, A. V.-H.-S. (2014). *The Risks of Nuclear Energy Technology-Safety concepts of Light Water Reactors*. Springer.

[19] Lee, H. (1980). Dynamic Characteristics of Fuel Rods. *Journal of the Korean Nuclear Society*.

[20] Gunnar Wikmark, L. H. (2009). Cladding to sustain corrosion, creep and growth at high burn-ups.

[21] W.V.Chaves, E. (2010). *University of Castilla la Mancha, Spain*. Recuperado el April de 2015, de https://www.uclm.es/profesorado/evieira/asignatura/meccomp/book/sistemas/integracion/integracion.pdf

[22] Rust, W. (2011). Nichtlineare Finite-Elemente-Berechnungen.

[23] P.Yvon, J. a. (1998). Irradiation Creep and Growth of Guide Thimble Alloys. France.

[24] Wanninger, A. (2015, February 9). Equivalence between creep laws linear and absolute values. Garching, Bayern, Germany.

[25] Whitmarsh, C. (n.d.). *Review of Zircaloy-2 and Zircaloy-4 properties relevant to N.S. Savannah reactor design*. Tennessee.

[26] Hengstler-Eger, R. M. (2012). Ion Irradiation Studies of the Origins of Pressurized Water Reactor Fuel Assembly Deformation. München, Bayern, Deutschland.

ANÁLISIS ESTRUCTURAL DEL SOPORTE DE UNA BARRA DE COMBUSTIBLE DE UN ELEMENTO DE COMBUSTIBLE DE UN PWR BAJO IRRADIACIÓN USANDO EL MÉTODO DE ELEMENTOS FINITOS

Ana
Alós
Díez